MICROFABRICATED DEVICE FOR TRANSDERMAL DRUG DELIVERY

A Thesis
Presented to
The Academic Faculty

by

Sébastien Henry

In Partial Fulfillment
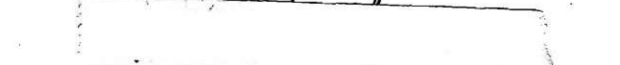of the Requirements for the Degree
Master of Science in Bioengineering

Georgia Institute of Technology
September 1997
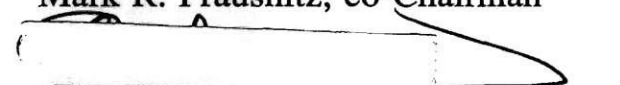
MICROFABRICATED DEVICE FOR TRANSDERMAL DRUG DELIVERY

Approved:

Mark G. Allen, co-Chairman

Mark R. Prausnitz, co-Chairman

Robert M. Nerem

Date Approved 8/8/97

ACKNOWLEDGMENTS

The company of my fellow graduate students in both my research groups was very enjoyable. I would like to thank them all for the good times. Special thanks go to Laure, Jennifer, David, J.B, and Chuck for their assistance and availability.

Last but not least, I would like to thank my parents for their constant moral support and all the rest.

TABLE OF CONTENTS

LIST OF FIGURES

SPV = Microspikes embedded in epidermis + 2V Voltage - SPRV = Microspikes inserted them removed + 2V voltage

SUMMARY

The work presented in this thesis has been completed as part of a broad project whose final goal is the development of a device for the transdermal delivery of drugs. The device would consist of hollow microneedles or plain microspikes mounted onto a drug reservoir. The development of such a device originates from the fact that transdermal drug delivery is a way of administering drugs that overcomes, to some extent, the limitations of oral delivery, the most common method of drug administration.

The black silicon method, a microfabrication technique, was used to produce arrays of silicon microspikes of, at most, a couple of hundred microns in height. The mechanical properties of microspikes were tested and shown to be excellent. Qualitative and quantitative experiments were run to assess the drug delivery capabilities of microspikes; in these experiments, arrays of sharp spikes were used to pierce epidermis, the outer layer of skin, enabling dye molecules (playing the role of drug molecules) to be transported across the skin barrier. Whereas the qualitative experiments suggested that microspikes could enhance transport of molecules, the quantitative experiments were designed to measure this transport. Using spectrofluorimetry, the transport of molecules across skin was measured under different conditions. The results demonstrated that microspikes, when coupled with a low voltage applied across epidermis, can enhance transport of dye molecules by a factor of up to 300. These results attest to the high potential of the drug delivery device that we want to develop.

CHAPTER I

INTRODUCTION

The administration of most drugs requires transport of the drug from outside the body into the systemic bloodstream. This is often achieved by swallowing the drug in pill form so that it enters the blood via the gastro-intestinal tract.

Presently, the most common method of drug administration, oral delivery, has three primary limitations: (i) the inability of many drugs to reach the bloodstream intact, due either to enzymatic degradation in the gastro-intestinal tract or liver, or to poor transport across the intestinal mucosa; (ii) limited control over the rate at which drug enters the bloodstream, usually resulting in a single, large dose; and (iii) poor patient compliance. In contrast, delivery through a needle (i.e., injection or continuous intravenous administration) provides a direct conduit into the body through which drugs can be administered intact at almost any rate. However, the use of needles suffers from other limitations, including pain, risk of infection, and requisite expertise in using needles.

In response, a large drug delivery industry has grown to develop other ways of administering drugs (Chien, 1991; Langer, 1990; Robinson and Lee, 1988). For example, transdermal drug delivery (Hadgraft and Guy, 1989; Kasting and Bowman, 1990; Smith and Maibach, 1995) has met with some success. In this approach, drug is delivered across the skin and into the bloodstream for systemic administration.

1

Because the main role of the outermost layer of skin, stratum corneum, is to hinder transepidermal water loss and penetration of foreign substances (Fartasch, 1996), passive delivery of hydrophilic drugs across the skin is extremely limited. This aspect of skin gave rise to the development of various transdermal delivery techniques whose common goal is to enhance the transport of substances through stratum corneum.

One of these techniques is the use of chemical enhancers; specific chemicals or combinations of chemicals are known to increase the transport of drugs across skin. Dimethylsulfoxide (DMSO), terpenes, oleic acid and azone are reported in the literature as efficient penetration enhancers. It is believed that some of these enhancers induce a disarrangement of the lipid bilayers of the stratum corneum while others act on the proteins (Bouwstra *et al*, 1991). Although chemical enhancers have proven to yield increased permeability of stratum corneum, they can also trigger skin irritation or other toxic effects which limit their use.

Biochemical enhancers are another type of chemical enhancer: the strategy behind the use of such compounds is the inhibition of specific lipid synthetic enzymes found in stratum corneum to render this dead-cell layer more permeable for longer periods of time. However, the potential application of biochemical enhancers *in vivo* in man remains to be thoroughly investigated (Guy, 1996).

Iontophoresis is another transport technique that uses an electric potential to enable the penetration of ionized molecules across skin by electrophoresis and non-ionized molecules by electroosmosis. Transdermal delivery of peptide drugs such as insulin, vasopressin and calcitonin has been achieved with iontophoresis. Many *in vivo* studies, including on humans, have been carried out. For example, the penetration rate of 6-carboxyfluorescein through the abdominal skin of a nude mouse by means of iontophoresis has been reported to experience a 16-fold increase compared to passive diffusion (Haga *et al*, 1996). However, the use of iontophoresis in transdermal drug delivery remains limited for two

key reasons: (i) iontophoresis lacks efficiency since only a small amount of the applied charge induces drug delivery, most of it being transferred by small ions such as Na^+ and Cl^- present in the body (Prausnitz et al, 1996); and (ii) iontophoresis may trigger local skin irritation (Smith and Maibach, 1995).

Electroporation is also being investigated as a transdermal drug delivery technique. Electroporation (or electropermeabilization) consists of causing temporary permeabilization of the outer layer of skin by creating aqueous pathways across lipid layers by means of short, high-voltage electrical pulses (Prausnitz et al, 1993). Large and small peptides, oligonucleotides and other drugs were transported across skin using electroporation; this transport has been shown in vitro to be controllable upon variation of the applied voltage and the number and duration of the pulses (Prausnitz et al, 1996) . A lot of work in the field of electroporation remains to be done in vivo in order to confirm the promising results obtained in vitro (Vanbever et al., submitted). This, added to the fact that little is known about the long-term effects of high-voltage electrical pulses on skin, suggests that the widespread use of electroporation as a therapeutic tool still belongs to the future.

Macromolecules have also been investigated as transport enhancers for skin electroporation. Although macromolecules do not enhance passive or iontophoretic transport, their use amplifies the efficacy of electroporation-induced transport by several orders of magnitudes. It has been shown that macromolecules increase transport via an interaction with skin when compounds are "carried" through stratum corneum by means of high voltages (Vanbever et al, 1997). Instead of increasing the disruption of the lipid bilayer of stratum corneum, like traditional chemical enhancers do, macromolecules stabilize the transient disorders caused by electroporation (Vanbever et al, 1997).

These novel approaches to drug delivery have the common goal of eliminating the need for needles because of the difficulties they cause (see below), even though needles provide the most controlled means of delivering drugs.

3

Unfortunately, because skin is a remarkably good barrier to transport, the above-mentioned techniques are presently all limited in their applications. Administration across mucosal tissues via the nasal, pulmonary, buccal, vaginal or other routes has also been explored, but has not yet found widespread application.

Another approach to drug delivery relies on a single conventional gauge needle mounted on a reservoir to deliver biotechnology products such as peptides or proteins and macromolecules across skin. One such device, being marketed by Elan Corporation as "Medipad", functions like a patch and is aimed at: (i) replacing syringes, pen injectors or jet injectors that are suitable for bolus-type delivery but not for continuous delivery (Meehan *et al*, 1996); (ii) replacing costly ambulatory infusion pumps that are used when continuous delivery or specific delivery (regular multiple doses for example) is required (Meehan *et al*, 1996); and (iii) enabling the patient to administer the drug to himself in a homecare situation (Meehan *et al*, 1996). Pre-clinical *in vivo* experiments carried out on the rabbit showed successful delivery of various compounds including insulin and salmon calcitonin. Successful delivery of low-molecular mass compounds as well as macromolecules over a 24-hour period was also achieved in human volunteers (Meehan *et al*, 1996). In this device, the needle has a height (from outer surface of the reservoir to the tip of the needle) of 0.3 to 3.0 mm, an outer diameter of 0.1 to 0.2 mm and an inner diameter of 0.05 to 0.075 mm (Meehan *et al*, 1996). The device that can deliver 1 to 10 ml of drug in a continuous fashion over a 48-hour period is small (5.5 cm in diameter and 1.1 cm thick), self-adhesive, and disc-shaped (Meehan *et al*, 1996). Discomfort, said to be minimal, was reported by volunteers who tried the device.

Taking an unprecedented approach, we propose to redesign the needle, creating a conduit which, like a conventional needle, has direct access to the body's interior, but, unlike a conventional needle, does not cause pain, poses no risk of infection, and requires

4

no expertise to use. This idea has been independently proposed by others (Gross, 1993; Gross and Kelly, 1996; Silicon MicroDevices, 1996), but no experimental results have been published in the scientific literature.

We propose to design a novel microfabricated needle which is user-friendly, infection free, and painless, thereby overcoming the limitations of conventional needles. Affixed to the skin, this device could deliver drugs continuously or intermittently for hours or days. Applications could include delivery of almost any drug, ranging from low-molecular weight compounds (e.g., fentanyl) to macromolecules (e.g., insulin).

The design of this new needle comes from an understanding of skin anatomy, which is discussed in the following chapter.

CHAPTER II

SKIN ANATOMY AND NEEDLE GEOMETRY

Barrier Function of Skin

Skin is made up of two distinctive layers, epidermis and dermis, epidermis being subdivided into stratum corneum and viable epidermis. The outer 10-15 μm of skin, called stratum corneum, is a dead tissue that forms the primary barrier to drug transport. Below lies the viable epidermis (50-100 μm), a tissue containing living cells, but devoid of blood vessels or nerves. Deeper still, the dermis forms the bulk of skin volume and contains not only living cells, but also nerves and blood vessels (Figure 1).

Stratum corneum can be considered as a two-compartment system composed of anucleate corneocytes, essentially made up of fibrous protein networks, and an intercellular matrix, mostly made up of neutral lipids organized in bilayers (Elias, 1988). The anucleate corneocytes form the bulk of stratum corneum. As for the intercellular matrix, it holds the anucleate corneocytes together.

The creation of the impermeable stratum corneum is the main role of viable epidermis. It consists of four cellular events: (i) keratinization, corresponding to the formation of the

6

principal fibrous proteins of the keratinocyte; (ii) keratohyalin deposition, responsible for the creation of histidine-rich protein, stratum corneum basic protein; (iii) synthesis of a highly cross-linked insoluble envelope surrounding the corneocyte; (iv) formation of neutral lipid-enriched intercellular domains (Elias, 1988). The first three stages of this process lead to the formation of the bulk of stratum corneum, the anucleate corneocytes. The last stage corresponds essentially to the synthesis of the intercellular matrix.
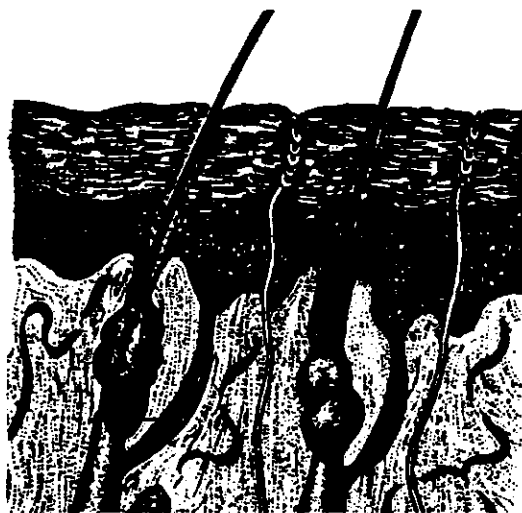
stratum corneum (10 μm thick)

viable epidermis (50 μm thick)

dermis (1 - 2 mm thick)

Figure 1: The Three Distinctive Layers of Skin.

The principal lipids of the intercellular matrix, thus of stratum corneum, are ceramides, cholesterol and fatty acids. These lipids are the product of the differentiation of the epidermal keratinocytes; they are arranged in multilamellar sheets and occupy most of the intercellular spaces of stratum corneum (Wertz, 1995). The free fatty acids represent 10-

15% of the stratum corneum lipid mass and the vast majority exhibits saturated straight chains. Their lengths vary between 14 and 28 carbons, 22 and 24 carbons, being the most common lengths (Wertz, 1995). Cholesterol accounts for about 25% of the stratum corneum lipid mass. As for ceramides, they are the most abundant lipids present in stratum corneum, accounting for 50% of the total lipids (Wertz, 1995).

Upon comparison of the lipids of stratum corneum found in mammals living on land and in water, it was found that ceramides and long-chain saturated fatty acids may constitute the barrier within stratum corneum (Elias, 1991), thus providing the outer layer of skin with its characteristic lack of permeability. The crucial role of cholesterol in the barrier function was also demonstrated in other experiments (Elias, 1991). These lipids that are necessary to maintain the barrier function are synthesized by epidermis, enabling stratum corneum to permanently prevent immoderate water loss and penetration of water-soluble substances from outside the body (Elias, 1991).

Needle Geometry

For transdermal drug delivery, once most compounds have crossed stratum corneum, transport through the viable epidermis and into the capillaries of the dermis occurs quickly. Therefore, a needle which is long enough to penetrate the stratum corneum, but short enough that it does not reach the nerves in the dermis, might provide a painless conduit for drug administration. Based on this, a device consisting of an array of needles which penetrate approximately <100 µm into the skin (Figure 2) would be a pain-free means of delivering drugs across skin. The device would be made up of a drug-containing housing

attached to silicon microneedles designed to transport drug across the poorly permeable stratum corneum without stimulating nerves in the dermis.

stratum corneum (10 μm thick)

viable epidermis (50 μm thick)

dermis (1 - 2 mm thick)
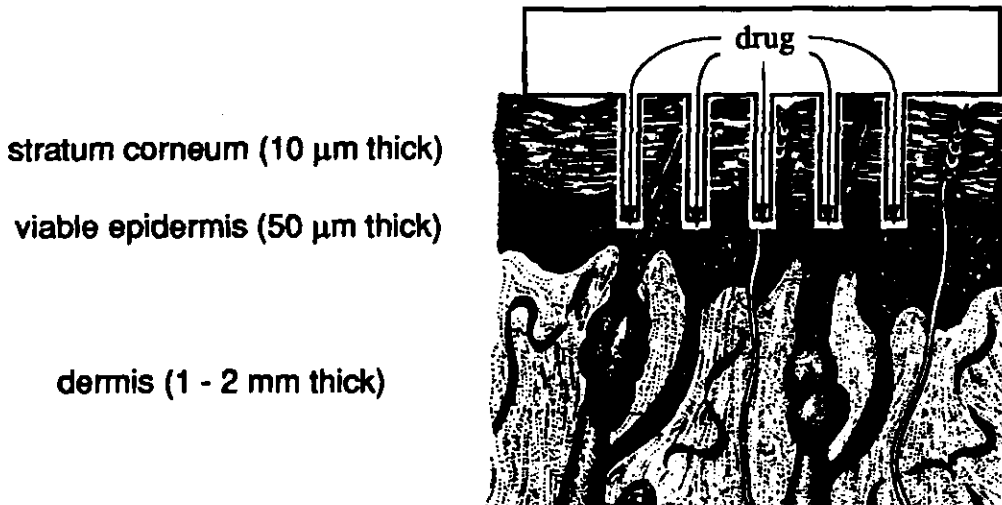
Figure 2: Device For Transdermal Drug Delivery.

A similar device but with a slightly different design may also allow transdermal delivery of drugs. In this case, the hollow microneedles are replaced by microspikes. Indeed, we think that microspikes that would be strong enough to pierce stratum corneum would create a hole in skin whose diameter would be larger than the diameter of the microspikes' bases; there would be enough space between stratum corneum and the microspikes for drug molecules to flow. A device consisting of microspikes mounted on a permeable reservoir should also be able to allow transdermal drug delivery (Figure 3). The microneedles or microspikes, like conventional needles or like the single gauge needle mounted on a reservoir used in the device, Medipad (Meehan *et al*, 1996), would create a pathway in

stratum corneum for drug molecules, enabling them to flow through the outermost layer of skin.

In this thesis, we focused on the fabrication of silicon microspikes as a means to enhance transport of molecules across stratum corneum.
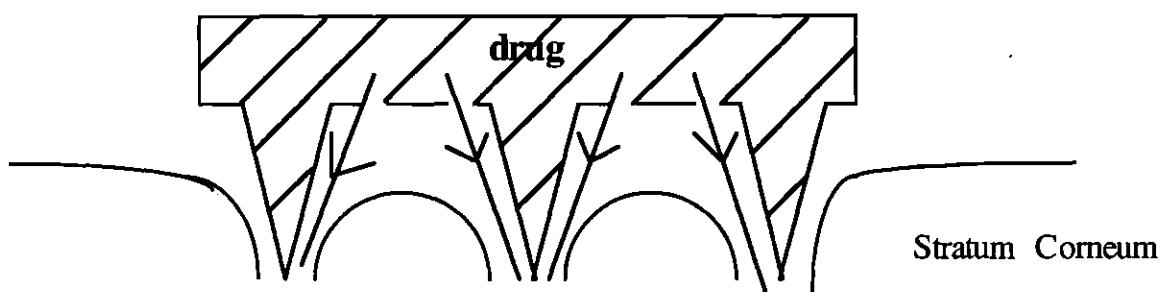
Figure3: Spikes Mounted On A Permeable Reservoir Making Holes In Stratum Corneum And Allowing A Drug To Flow Through These Holes.

A study was performed on the biocompatibility of silicon microelectrodes similar in size and shape to the structures we want to microfabricate. In this study, biocompatibility issues with respect to the design of inserted microelectrode arrays in neural tissue were addressed (Edell *et al.*, 1992). It is reported in this study that the design of insertable microelectrode tips has historically used conically-shaped micropipets or microwires because the hole made in tissue by such a microscopic tip is minuscule. However, when used in fragile tissue, conically-shaped structures can have harmful effects. Indeed, as conically-shaped microelectrode tips are pushed into a fragile tissue, the nearby tissue is pushed away

10

(without being cut) and only a small area of the tissue is severed (Edell *et al.*, 1992). The surrounding tissue, that undergoes only pushing, stretches and then forms strips along the tip. Further insertion of the microelectrodes into the tissue renders the strips larger and tighter. Because of this phenomenon, the strips need more force to slip along the tip. Additional force on the advancing tip spreads to adjacent tissues as the strips compact (Edell *et al.*, 1992). The tissue in the surroundings of the strips is pulled into tension and breaks if the tension exceeds its elastic limits (Edell *et al.*, 1992). This can also result in the rupture of nearby blood vessels leading to microhemorrhages (Edell *et al.*, 1992).

Although the conical design does not seem to be the most suitable design in the case of the very fragile neural tissue (the chisel-point design seems more appropriate), it is certainly a good, if not the best, design for skin piercing purposes. Indeed, when the tissue to be pierced is homogeneous and elastically deformable, such as skin, the holes made by conically-designed piercing structures are small and, upon further insertion, the tissue is smoothly moved away form the tips of the piercing structures (Edell *et al.*, 1992). Therefore, for our application, we decided to fabricate arrays of conically-shaped microspikes. Such arrays can be made by means of microfabrication techniques.

Once affixed to the skin, our device should cause, at most, minor reactions from the patient's body. Ideally, the silicon microspikes should not be seen by the patient's antibodies as foreign agents. Therefore, the biocompatibility of silicon is a main concern in our work.

Those studies have been reported on silicon biocompatibility all indicate that inserted silicon structures, under certain conditions (shape, size, etc.), are fairly well accepted by the human body.

CHAPTER III

MICROFABRICATION

Microfabrication technology was used to make microspikes of micron dimensions because using this technology it is possible to make such structures easily, cheaply and reproducibly.

Historical Perspectives

Microfabrication is the technology used to fabricate computer chips. It has grown rapidly in the last three decades and nowadays permits mass production of devices having dimensions as small as nanometers. The first successful fabrication techniques produced single transistors on a silicon die 1 to 2 mm on a side. Early integrated circuits included several transistors and resistors to make simple logic gates and amplifier circuits. From this modest beginning, integration levels of several million components on a 7 mm × 7 mm die have been reached (Jaeger, 1993).

To realize the progress of silicon microelectronics it is easiest to take the example of memory chips. Memory chips are extremely regular and can be sold in large volumes, making technology customization for the chip design economical. As a result, memory

chips have the highest density of all integrated circuits. For example, a one-megabit dynamic random-access memory (DRAM) has more than 2 million components per chip of millimeters dimensions (Campbell, 1996). One of the most fundamental changes in the fabrication process that allows such high integration levels is the minimum feature size that can be printed on a chip. Over the last 25 years, integrated circuits have progressed from tens of microns to tens of nanometers (Campbell, 1996).

Germanium was one of the first materials to receive wide attention for use in microfabrication of electronic components, but it was rapidly replaced by silicon during the early 1960s (Campbell, 1996). Silicon emerged as the dominant material because it was found to have major processing advantages. Silicon can easily be oxidized to form silicon dioxide. Silicon dioxide was found to be not only a high-quality insulator but also an excellent barrier layer for the selective diffusion steps needed in integrated-circuit fabrication (Jaeger, 1993). Silicon was also shown to have a number of additional advantages. It is a very abundant element in nature, providing the possibility of a low-cost starting material. It can operate at higher temperatures than germanium without undergoing degradation. It appears that the processing advantages were the dominant reasons for the emergence of silicon over the other semiconductor materials (Jaeger, 1993).

Early fabrication used silicon wafers which had 1- and then 2-inch diameters. The size of the wafers has steadily increased to the point where 4-, 5-, and 6-inch wafers are now in production. Wafers with 8-inch diameters have also been successfully produced by silicon wafer manufacturers (Jaeger, 1993). The larger the diameter of the wafer, the more integrated-circuit dice can be produced at one time because the same silicon chip is replicated as many times as possible on a silicon wafer of a given size. Since many wafers are processed at the same time and since processing costs per wafer are relatively independent of wafer size, the cost per die is lower for larger wafer sizes. Thus, there are

strong economic forces driving the integrated-circuit industry to continually move to larger and larger wafer sizes (Jaeger, 1996).

Deep Plasma Etching

Deep plasma etching is the fabrication technique that we used to create silicon microspikes, which are structurally regular and mechanically robust. In the deep plasma etching process, also known as the reactive ion etching process, an appropriate masking material (e.g., metal) is deposited onto a silicon wafer substrate and patterned into dots having the diameter of the desired microspikes. The wafer is then loaded into a reactor chamber, a reactive ion etcher (RIE), and subjected to a carefully controlled plasma based on fluorine/oxygen chemistries to etch very deep, high aspect ratio[1] trenches into the silicon. Those regions protected by the metal mask remain and form the spikes.

To obtain the desired high aspect ratio structures (microspikes), the Black Silicon Method (BSM) can be used (Jansen *et al.*, 1995). This method, a deep plasma etching process, receives its name because silicon appears black when it is etched exactly anisotropic (the vertical etch rate is much greater than the horizontal etch rate).

To perform the BSM, an $SF_6/O_2/CHF_3$ plasma is needed. In such a plasma, each gas has a known specific function and influence, so the etched profile is easily controlled just by changing the flow rate of one of these gases. Within the plasma, (a) SF_6 produces the F^* radicals for the chemical etching of the silicon forming the volatile SiF_4, (b) oxygen creates the O^* radicals to passivate the silicon surface with SiO_xF_y, and (c) CHF_3 (or SF_6)

---

[1] The aspect ratio of a structure is defined as the height of this structure over its width (height/width).

is the source of CF_X^+ (or SF_X^+) ions, responsible for the removal of the SiO_XF_y layer at the bottom of the etching trenches forming the volatile $COxFy$ (or $SOxFy$) (Figure 4).
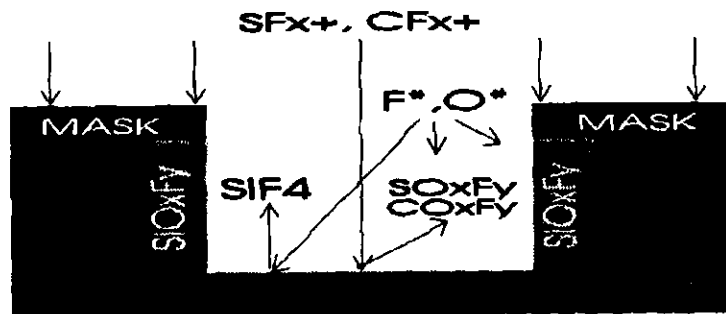
Figure 4: The $SF_6/O_2/CHF_3$ Chemistry (Jansen et al., 1996).

Plasma (Figure 5)

Once the silicon wafer is loaded inside the reactor chamber, the gases used to etch the silicon are allowed to enter the chamber where they are mixed and then subjected to a radio-frequency (rf) voltage to form a plasma (Jansen et al., 1996). The reactor chamber consists of two electrodes connected to an rf voltage source that encloses a low pressure gas as a dielectric. The rf electric field will force electrons to the positive electrode. In their way they will collide with the feed gases (eg., SF_6, O_2, CHF_3) generating the gas phase etching environment which consists of neutrals (N), radicals (R), electrons (E), ions (I), photons (P) and phonons (T). The photons are responsible for the characteristic glow of the plasma. Since the electron mobility is much greater than the ion mobility the electrons are able to track the rf electric field. After ignition of the plasma, the electrodes acquire a negative

charge whereas the plasma becomes positively charged. Of course, only electrons in the direct neighborhood of the electrodes will reach them during the rf cycle. Therefore, a thin region depleted from electrons will be developed close to the electrodes: the plasma sheath. Because there are no electrons in this region to generate photons, the region is dark and the plasma sheath is also known as the dark space. The rest of the plasma is called the glow region. Both regions are separated clearly by the so-called boundary layer. Shortly, a plasma can be divided into three components: i) the glow region full of electrons, ii) the sheath region depleted from electrons, and iii) the boundary layer separating both regions. Due to the charging of the glow region, a dc electrical field will exist in the sheath region forcing positive ions to the electrode. This phenomenon is typical for reactive ion etching: a continuous flow of directed ions together with an isotropic flux of radicals. In most cases, the area of the two electrodes facing the plasma are not the same. Therefore, a different negative charging of the electrodes is a result and the dc voltage between the glow and one of the electrodes will differ from the other one. This difference in dc voltage between the two electrodes is called the dc self-bias which is a measure of extreme importance in reactive ion etching. The electrode having the biggest area facing the plasma is always at a higher dc potential than the smaller one and is called the anode. The smaller electrode is known as the cathode (Jansen *et al.*, 1996).
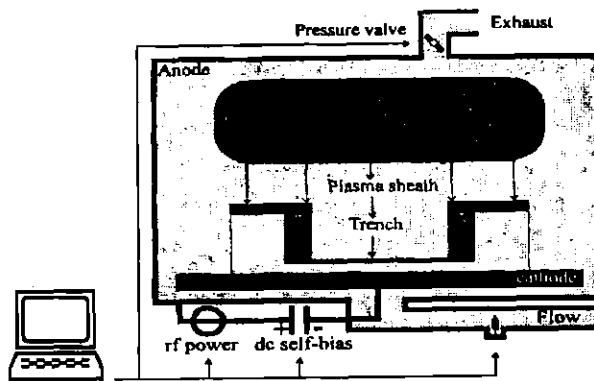
Figure 5: Basic RIE System (not drawn to scale).

The Glow Region

The electrons gain energy from the rf power source. Generally, the electrons will collect energy between 3 and 30eV before colliding with another particle; this is strongly depending on the operation pressure of the RIE. A typical particle generated by electron impact is the photon. The energy of the photon depends on the electronic configuration of the bombarded particle (Jansen *et al.*, 1996). The total spectrum of photons gives the plasma a typical color. For example the color of an SF_6/O_2 plasma is purple.

The Boundary Layer

The energetic particles from the plasma glow should be transported to the sample (to be etched) surface. This is accomplished by a flux of particles through the plasma boundary layer. The radicals have only thermal energy and leave the surface in all directions (i.e. isotropically). However, because the glow is a conductor, the electric field is pointing perpendicular to the boundary surface and the ions leave the boundary layer at an angle of 90 degrees (Jansen *et al.*, 1996).

The Sheath Region

Both radicals and ions will collide with gas particles during passing the sheath. Especially the effect of the pressure on the ions is crucial. Because of the collisions of ions with other particles, ion dispersion will occur (i.e., their direction will not exactly correspond with the normal of the boundary layer anymore). At the same time, the energy of the ions is exchanged with the particles. The rf frequency is responsible for a varying plasma potential. So, the energy of an ion depends on the time that the ion enters and leaves the boundary layer.

In most cases, the collision of radicals with other particles is not important because, generally, this flux is already isotropic. However, during extensive silicon etching there will be a continuous net flow of radicals from the non-etching surrounding to the etching area (Jansen *et al.*, 1996).

Origin of Black Silicon

The flux of particles from the $SF_6/O_2/CHF_3$ plasma glow region is used to etch samples (silicon in our case). There is a constant competition between the fluorine radicals that etch and the oxygen radicals that passivate the silicon. At a certain oxygen content there is such a balance between the etching and the passivation that a nearly vertical wall results. At the same moment native oxide, dust and other small particles will act as micro masks and, because of the directional etching, spikes will appear (Figure 6). These spikes consist of a silicon body with a thin passivating siliconoxyfluoride skin and are of poorly

controlled geometry because of the random size and shape of their masks. If the length of the spikes exceeds the wavelength of incoming light, this light will be "caught" in the areas between the spikes and the silicon surface appears black. The origin of micro masks is caused by native oxide, dust, and so on which is already on the wafer before etching, but they are also formed during the etching because silicon oxide particles coming from the plasma adsorb at the silicon surface or because of the oxidation of the silicon surface together with the angle dependent ion etching of this oxide layer. Another source of particles during etching which will act as micro masks is the resputtering of mask material due to imparting ions (Jansen *et al.*, 1996).

The literature provides a method that allows to make black silicon using either *in situ* micromasks or deposited metal masks of controlled geometry (Jansen *et al.*, 1995). The microfabrication technique that we utilized to make microspikes is based on this method; we used deposited metal masks of microns dimensions.

Figure 6: Black Silicon Spikes (Jansen *et al.*, 1995).

Cleanroom

To make spikes of microns dimensions, it is necessary to use microfabrication techniques. This implies that the working environment has to be ultra clean. Indeed, for example, a piece of hair measures about 80 microns in diameter which is larger than the base diameter of the microspikes we fabricated! Therefore, in a regular working environment, the samples (silicon wafers), while being processed, would be progressively covered by hair, dust et cetera making impossible the microfabrication of spikes.

The ideal would be to work in a particle-free environment. Although it is not possible to reach such a degree of cleanliness, it is feasible to microfilter the ambient air to

considerably decrease both the number and size of the particles: a cleanroom is used for this effect. In our laboratory, the cleanroom is divided into two different areas: the class 10 area and the class 1000 area. The class 10 area is defined as having fewer than 10 particles of more than 0.5 micron in size within a cubic foot (ca $0.0283m^3$) of air. Similarly, the class 1000 area has fewer than 1000 particles of more than 0.5 micron in size within a cubic foot of air. To obtain such an almost-particle-free environment, the air inside the cleanroom is constantly filtered; the users are required to wear special clothing (gown) and to respect procedures and policies listed in appendix I.

CHAPTER IV

REACTIVE ION ETCHING

A reactive ion etcher, RIE, was used to fabricate microspikes. Two 2-inch silicon wafers were loaded at a time in a RIE in which they were subjected to a plasma based on fluorine and oxygen chemistries. The fabrication of microspikes exhibiting different heights and profiles was made possible by adjusting the different parameters (power, pressure, gas flow rates, silicon loading).

Materials and Methods

The reactor chamber, RIE, (700 series waf'r/batch Plasma Processing System, Plasma Therm, Inc., St. Petersburg, FL, USA) available in our cleanroom contains four plates that have a 4-inch diameter each. It is possible to process four silicon wafers of, at most, 4 inches (10.16 cm) in diameter at a time. Four gas bottles can be hooked up to the reactor chamber allowing the operator to run experiments with a mix of four different gases. In our case, only three gases are necessary: SF_6, O_2 and CHF_3. The operating pressure, power and gas flows can be adjusted by the user.

We used <100>-oriented, prime grade, 450-550 μm thick, 10-15 Ω-cm silicon wafers (Nova Electronic Materials Inc., Richardson, TX, USA); different diameters were tried: 2,3 and 4 inches (5.08, 7.62 and 10.16 cm).

For the process itself, we followed the following Black Silicon Method found in the literature (see appendix 2). Because the RIE that we use is set up differently from the one used by the authors of the original Black Silicon Method (Jansen *et al.*, 1995), the operating parameters had to be adjusted accordingly.

Power

The Black Silicon Method recommends 1 W/cm^2: since our machine contains 4 plates of 4 inches in diameter each, the power should be set at 324 W to achieve the same power density but we are limited by our machine to a power of 250 W. That is the power that we initially used.

Pressure

The pressure mentioned in the Black Silicon Method was initially used: 100 mTorr.

Gas flows

The Black Silicon Method recommends to start running experiments with an initial flow of 100 sccm for SF_6 and of 1 sccm for O_2 but it is important to understand that, to make microspikes, the SF_6/O_2 ratio is much more important than the flows themselves: the recommended flows correspond to an SF_6/O_2 ratio of 100. As for CHF_3, no specific flow is suggested. With our RIE, the maximum flow available was 30 sccm for all the gases hooked up to the reactor chamber. We investigated a range of different SF_6/O_2 ratios between 1 and 2.

Silicon Loading

The silicon loading refers to the area of etchable silicon inside the reactor chamber: for a certain SF_6/O_2 ratio, if the etchable silicon area is increased (by switching to a larger silicon wafer, for example), the concentration of gas molecules/cm^2 of silicon will decrease, altering the overall effect of the gases on the silicon wafers.

The Black Silicon Method is not specific about the amount of silicon to insert into the RIE. However, once gas flow rates, pressure, and power have been set, it is suggested to place a piece of silicon inside the RIE, start etching and increase the silicon loading until black silicon is formed. We followed the approach as described below.

RIE Cleaning

The Black Silicon Method is a very sensitive process; as such, it can be altered by slight contamination present inside the reactor chamber, which can prevent black silicon formation. Since our reactor chamber is operated for a variety of different purposes by multiple users who run different gases, contamination occurs every time someone utilizes the reactor chamber. The inside of the chamber gets coated, both by a thin layer of gas particles and by material etched off the wafer(s), after each run. If the contamination is not removed before we start our experiments, then the O_2, which is needed for the black silicon formation, can react preferably with the contaminants, thus impairing the black silicon process. To overcome this problem, cleaning of the reactor chamber before each run has to be performed. First, the chamber is cleaned mechanically, using a cleanroom paper towel soaked with isopropanol, to remove particles etched off wafers. Second, a mix of O_2 and CHF_3 (10:1) is run for 15 minutes to remove the contaminants that were not taken care of by the mechanical clean. Third, pure O_2 is run for 45 minutes to remove contamination

directly caused by the gases themselves. High pressure (400 mTorr) and power (300 Watts) are applied during the cleaning steps performed with gases in order to maximize the cleaning effects.

Wafer Cooling

It is important to ensure very good thermal contact between the wafers and the cathode of the RIE; keeping the wafers' temperature constant while etching is crucial to obtain black silicon. Although a cooling liquid flows underneath the cathode, it is not sufficient by itself to prevent the wafers from warming up during the process. To keep the wafers' temperature constant during the etch, vacuum grease has to be spread on the backside of the wafers, prior to placing them on the cathode, in order to enhance the heat transfer from the wafers to the cathode.

Setting Parameters

SF_6/O_2 Ratio and Loading

According to the Black Silicon Method, two parameters are of extreme importance: the SF_6/O_2 ratio and the loading. Since it is essential to control these two parameters, the minimum loading necessary to obtain black silicon had to be determined. We started operating at a low SF_6/O_2 ratio that would have enabled us, for sure, to get some black silicon provided that the loading had been sufficient. The SF_6 and O_2 flows were respectively set at 20 and 10 sccm, resulting in a SF_6/O_2 ratio of 2. Different loadings were subjected to this SF_6/O_2 ratio for 10 minutes. The running time was set at 10 minutes because the Black Silicon Method suggests that etching at least about 1 micron of silicon is sufficient to obtain black silicon provided that all the parameters are correctly set; we

25

estimated that 10 minutes would be enough to etch at least 1 micron of silicon even for a loading of four 4-inch wafers, which is the maximum capacity of our RIE.

Performing a cleaning of the chamber before each run and using vacuum grease (Apiezon N, K.J. Lesker Co., Clairton, PA, USA) on the backside of the wafers, we tried different loadings ranging from a single 2-inch wafer to four 3-inch wafers for 10 minutes. Vacuum grease was also applied on some parts of the top side of the wafers which shielded areas on the silicon wafers, preventing these areas from being etched. In these conditions, we found that two 2-inch wafers yielded structures with the highest aspect ratio (Figure 7).

Pressure and Power

After selecting the right SF_6/O_2 ratio (20/10) as well as the right loading (two 2-inch wafers), we fine tuned pressure and power and obtained the best results (largest aspect ratio) for the following values:

Pressure = 150 mT

Power = 180 W
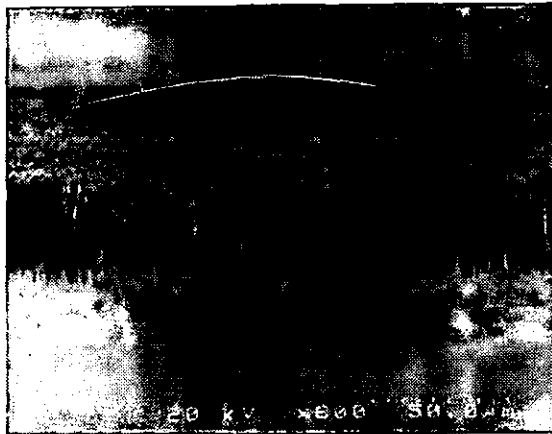
- - - - - - - - - ~50 μm

Figure 7: High-Aspect-Ratio Structures Obtained With A Loading Of Two 2-Inch Wafers. Vacuum Grease Was Used As A Masking Material.

The fact that our SF_6/O_2 ratio seems extremely low compared to what is suggested in the Black Silicon Method is not surprising. It is well known that it is possible to obtain the same results with very different settings when different RIEs are used.

These initial results showed that CHF_3, which is recommended in the Black Silicon Method, was not necessary for the fabrication of high-aspect-ratio structures. As shown later, these results were confirmed by other experiments.

Masking Material

We opted for metal as a masking material. Unlike vacuum grease, some metals are very resistant to plasmas and they are very easily patterned into almost any shape or size. Using

27

basic microfabrication techniques, we deposited a metal layer on wafers and patterned it into arrays of dots.

Patterning Metal (Figure 8)

A metal of choice, in our case chromium (see below), is first deposited onto a silicon wafer. The metal layer is then patterned into dots by means of photolithography. Photolithography is an optical printing method which is used to transfer geometric patterns, usually generated with a computer, from a negative, or mask, onto a surface.

After the geometric patterns are designed by computer, they are transferred onto a glass plate, covered with a thin emulsion layer, during a photo-reduction step. The glass plate is called the mask. In our case, the pattern on the mask consists of arrays of black dots on a transparent background.

Once the mask is ready, a layer of photosensitive material, 1827 photoresist (Shipley, Marlborough, MA, USA), is deposited onto the metal layer covering the silicon wafer.

Then, the mask is carefully positioned on top of the photoresist layer and UV light is shined through the mask. Photoresist is exposed wherever metal (lying underneath the photoresist layer) needs to be removed; it is developed with a process very similar to that used for developing ordinary photographic films by means of a liquid developer, 354 developer (Shipley, Marlborough, MA, USA). Photoresist is removed wherever the exposing light passes through the mask, leaving bare metal in the exposed areas. A photoresist acting in the manner just described is called a positive photoresist and the mask contains a copy of the pattern which will remain on the surface of the wafer.

In a subsequent step, the wafer is dipped into a chemical solution that etches the metal that was exposed by photolithography, leaving dots of metal on the silicon wafer's surface.

These dots of metal are also called masks and in the remainder of this thesis, *masks* will refer to these metal dots.

Finally, the photoresist still present on the dots of metal is removed with a solvent. The result is that the silicon wafer is covered by metal masks in a pattern of dots. The metal dots will cover the sites where microspikes will be created.

Metal Deposition

Photoresist Deposition

Photoresist Patterning

UV Light

Photoresist Development

Metal Etching

Photoresist Removal

Silicon Etching
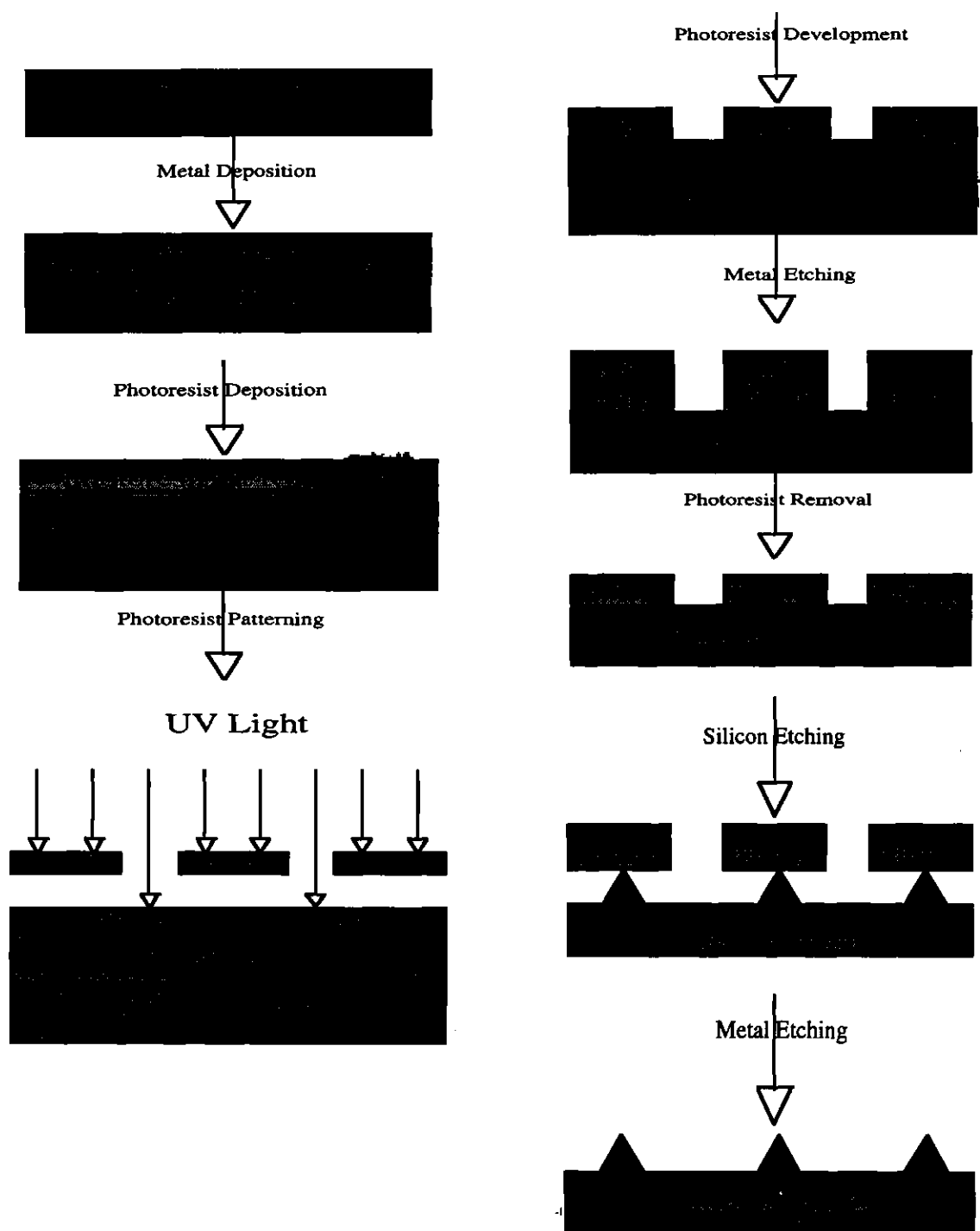
Metal Etching

Figure 8: Steps, Including Metal Patterning, Followed In The fabrication Of Microspikes.

Metal Choice

The choice of the metal is driven by the silicon/metal selectivity during the plasma etching of silicon. The silicon/metal selectivity refers to the ability of the metal to remain intact while silicon is being etched. Although there exist many different metals to choose from, only a few, according to the available literature, can actually resist, and only to a certain extent, the plasma used to etch silicon.

A study (Jansen, 1996) shows that the following metals do not resist fluorine-based plasmas well:

- aluminum

- gold

On the contrary, the following metals can resist fluorine-based plasmas well:

- chromium (said in the study to be ideal)

- nickel (said to be as good as chromium)

- copper (said to give good results, although not as good as chromium or nickel)

- palladium (said to be OK)

Based on these recommendations we tried chromium, nickel and copper. We found that the silicon/nickel and silicon/copper selectivities are actually poor (nickel and copper are etched along with silicon in fluorine-based plasmas). However, our experiments confirmed that the silicon/chromium selectivity is better than both the silicon/nickel and silicon/copper selectivities, which led us to use chromium.

31

Results

Sharp microspikes exhibiting different aspect ratios were fabricated using chromium masks. This was made possible by altering the SF_6/O_2 ratio, thus controlling the underetch of the chromium masks.

Several 16 by 16 arrays of 50-μm-Cr dots were deposited onto two 2-inch wafers that were later placed into a reactor chamber and subjected to an SF_6/O_2 plasma. The different parameters were set to values identical to those which had allowed us to get high-aspect-ratio structures when vacuum grease was used as a masking material:

SF_6 flow: 20 sccm

O_2 flow : 10 sccm

Pressure: 150 mT

Power: 180 W

These parameters yielded almost-straight "poles" of silicon. Figure 9 shows a silicon pole that was obtained after a 50-minute run; the silicon poles were about 45 μm tall and 10 μm wide, corresponding to an aspect ratio of 4.5: the mask is still present, lying on top of the pole. These first results confirmed that we had found a set of parameters which etches high-aspect-ratio structures.

Mask

Silicon   Pole

Silicon   Substrate

- - - - - - - - - - ~10 μm
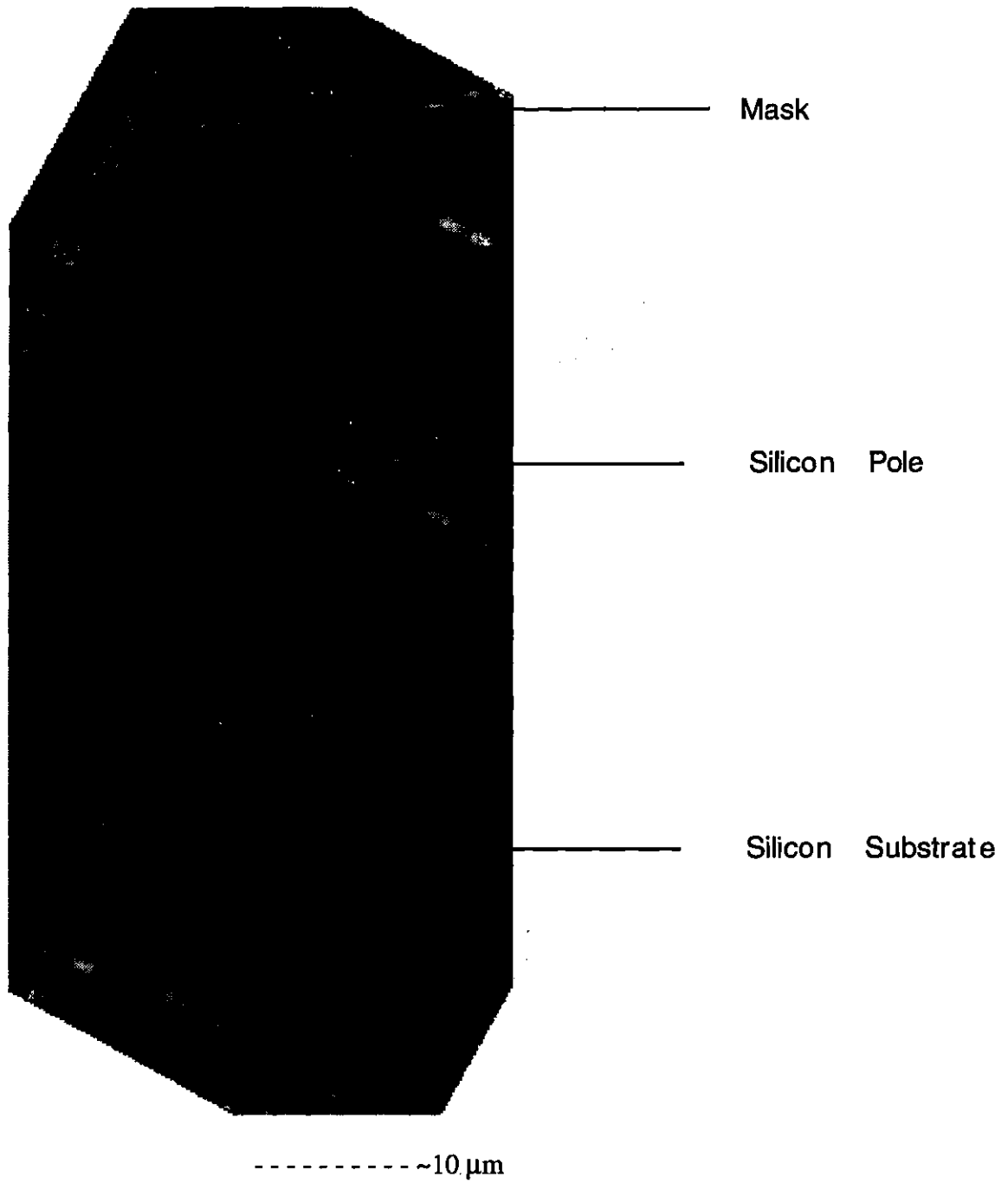
Figure 9: Scanning Electron Micrograph of An Almost-Straight Pole Of Silicon With The Mask Still In Place On The Top.

Two phenomena taking place during the etching of the structures were noticed. First, the chromium masks are altered during the process; indeed, they are etched on the edges and fold over themselves (Figure 9). However, this mask degradation is very slow and, as we will see later, we managed to take advantage of it. Second, underetching occurs during the process (silicon is removed under the masks); instead of etching purely straight down, the plasma also etches horizontally under the masks which narrows the silicon poles. We also took advantage of this phenomenon in the subsequent experiments.

The next step in the fabrication process consisted of modifying the parameters in order to obtain sharp spikes instead of straight poles. From the Black Silicon Method (Jansen *et al.*, 1995), we learned that pressure and power have an influence on the profile of the etched structures. First, we varied pressure and power without changing the SF_6 and O_2 flows, but we did not notice any significant change in the shape of the etched structures. This might have been because the influence of pressure and power on the profile of the etched structures may depend on the gas flows. Therefore, we set pressure and power back to their initial values and started focusing on the gas flows. It is known that changing the O_2 flow rate can alter the profile of the structures (Jansen *et al.*, 1995). Once parameters allowing the formation of straight high-aspect-ratio structures are found, it is possible to render the structures positively tapered (base wider than tip) by increasing the O_2 flow or negatively tapered (tip wider than base) by decreasing the O_2 flow. Since the first set of parameters yielded slightly negatively tapered structures (Figure 9), the O_2 flow was increased in order to get positively-tapered spikes. We increased the O_2 flow to 15 sccm without modifying the other parameters. Figure 10 shows spikes obtained with a 15-sccm O_2 flow after a 130-minute run; it confirms that the chromium masks shrink during the etch and it shows that the etch in the horizontal direction is more pronounced at the tip of the structures than at their base thus yielding a positively-tapered profile. During longer runs, the masks eventually stop shrinking but the mask underetch goes on, which sharpens the

34

structures even more; at some point, the structures become so sharp that the masks fall off, leaving well-defined sharp spikes. Figure 11 shows an example of such spikes: they reached a 140-μm height after a 140-minute run.

As expected, the increase in O_2 flow resulted in the formation of very tall and positively tapered structures. Also, these results showed that the shrinking of the chromium masks during the etching of the spikes is not a problem. Since our experiments confirmed that O_2 flows greater than 10 sccm had a desirable effect on the spikes' profile, we kept investigating this effect. Therefore, the O_2 flow was raised to 17.5 sccm; all the other parameters remained unchanged.
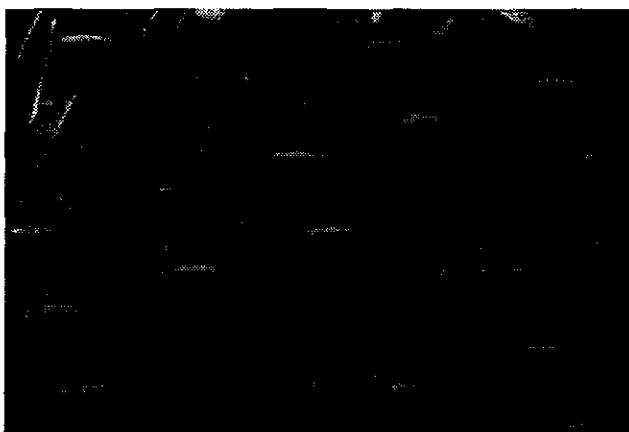
- - - - - - - - - - - - ~136 μm

Figure 10: Scanning Electron Micrograph Of Spikes With Their Masks Still In Place.

Spikes' height: ~ 135 μm   *Pressure: 150 mT*

SF$_6$/O$_2$ ratio: 1.33   *Power: 180 W*

Loading: two 2-inch wafers   *Running time: 130 min*

Masks' diameter: 50 μm
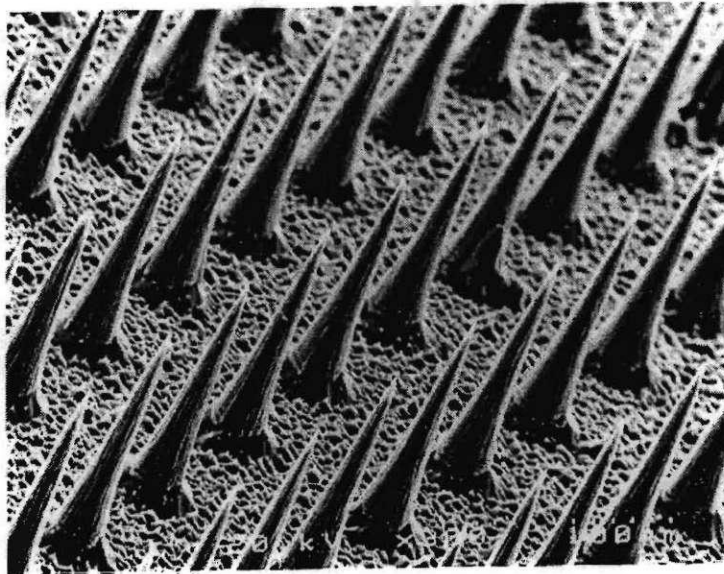
- - - - - - - - - - - ~100 μm

Figure 11: Scanning Electron Micrograph Of Spikes After Complete Underetch Of Their Masks.

Spikes' height: ~ 140 μm

Aspect Ratio: ~3

SF$_6$/O$_2$ ratio: 1.33

Loading: two 2-inch wafers

Pressure: 150 mT

Power: 180 W

Running time: 140 min

Masks' diameter: 50 μm

As expected, the 17.5-sccm O_2 flow yielded more-positively-tapered (lower aspect ratio) structures compared to those obtained with a 15-sccm O_2 flow. Figure 12 shows 80-

36

μm spikes obtained with a 17.5-sccm O_2 flow after a 120-minute-run. Similar to what happens with a lower O_2 flow, the chromium masks shrank during the etch and finally fell off the sharp spikes. The effect of a 20-sccm O_2 flow (the other parameters remaining unchanged) on the spikes' profile was also investigated. The spikes made under these conditions are even more positively tapered. Figure 13 shows 40-μm spikes that were fabricated in 90 minutes.

- - - - - - - - ~75 μm

Figure 12: Scanning Electron Micrograph Of Spikes.

Spikes' height: ~ 80 μm	*Pressure: 150 mT*
Aspect Ratio: ~2	*Power: 180 W*
SF_6/O_2 ratio: 1.14	*Running time: 120 min*
Loading: two 2-inch wafers	*Masks' diameter: 50 μm*

The differences in profiles induced by increasing the O_2 flow is easily noticeable, especially at the spikes' base where the profile is pyramidal (this disruption of the profile line at the base of the spikes is not well understood but we assume that it is due to the arrangement of the crystallographic planes in the silicon). As the O_2 flow increases, the etch profile becomes more and more positive, which leads the chromium masks to be totally underetched faster; this causes the etching time and the spikes to be shorter.

- - - - - - - - - ~30 μm

Figure 13: Scanning Electron Micrograph Of Spikes.

Spikes' height: ~ 135 μm	*Pressure: 150 mT*
Aspect Ratio: ~1	*Power: 180 W*
SF_6/O_2 ratio: 1	*Running time: 130 min*
Loading: two 2-inch wafers	*Masks' diameter: 50 μm*
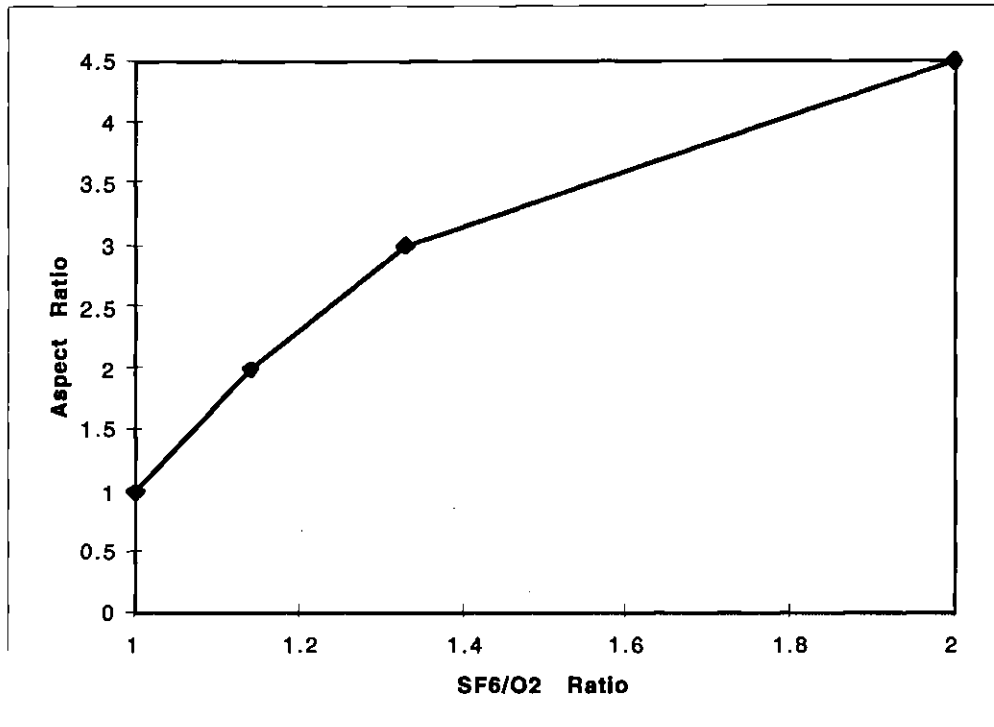
Figure 14: Effect Of The SF_6/O_2 Ratio On The Microspikes' Aspect Ratio.

These results show that, upon increasing the O_2 flow, the spikes' aspect ratio is decreased (figure 14). More than the O_2 flow itself, it is the SF_6/O_2 ratio which is of importance. If an SF_6/O_2 ratio equal to 1 gives a certain profile, it is possible to obtain the same profile whatever the SF_6 and O_2 flows are, provided that their ratio is 1. However, for a given ratio, the higher the SF_6 and O_2 flows, the higher the etch rate (Figure 15).
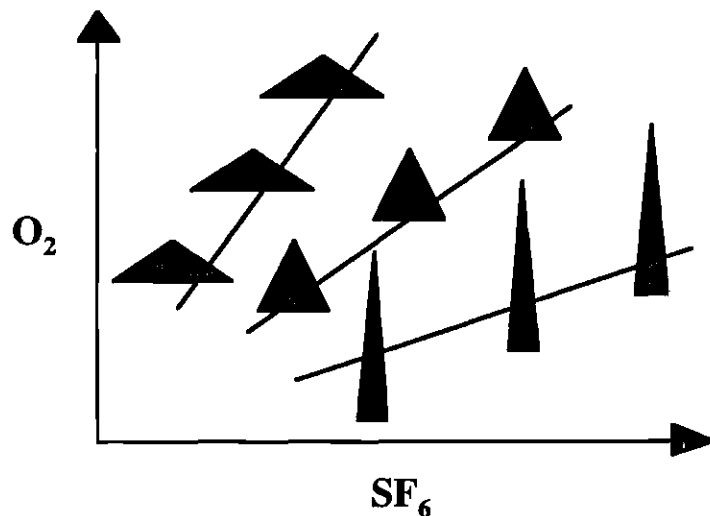
Figure 15: Influence Of The SF_6 And O_2 Flows On The Spikes' Profiles And Etch Rates.

- *If the SF_6 and O_2 flows are increased while the SF_6/O_2 ratio remains constant, the profile of the etched spikes is not altered but the etch rate increases.*

- *If the SF_6/O_2 ratio is increased, the profile of the spikes becomes more positively tapered.*

Once we managed to microfabricate spikes, we tested them in order to study their ability to pierce skin and to enhance the transport of molecules across it. Among all the different spikes we made, we decided to use those that had the highest aspect ratio (obtained with an O_2 flow equal to 15 sccm) for several reasons. First, they were the tallest, which made them the best candidates to ensure complete piercing of the stratum corneum (from top to bottom). Second, because they were more narrow, they may have damaged the skin less as suggested (Edell, 1992). 80-µm-chromium masks were also used

to make larger microspikes that were ~180 μm tall (Figure 16); these microspikes were used in the experiments run on skin.
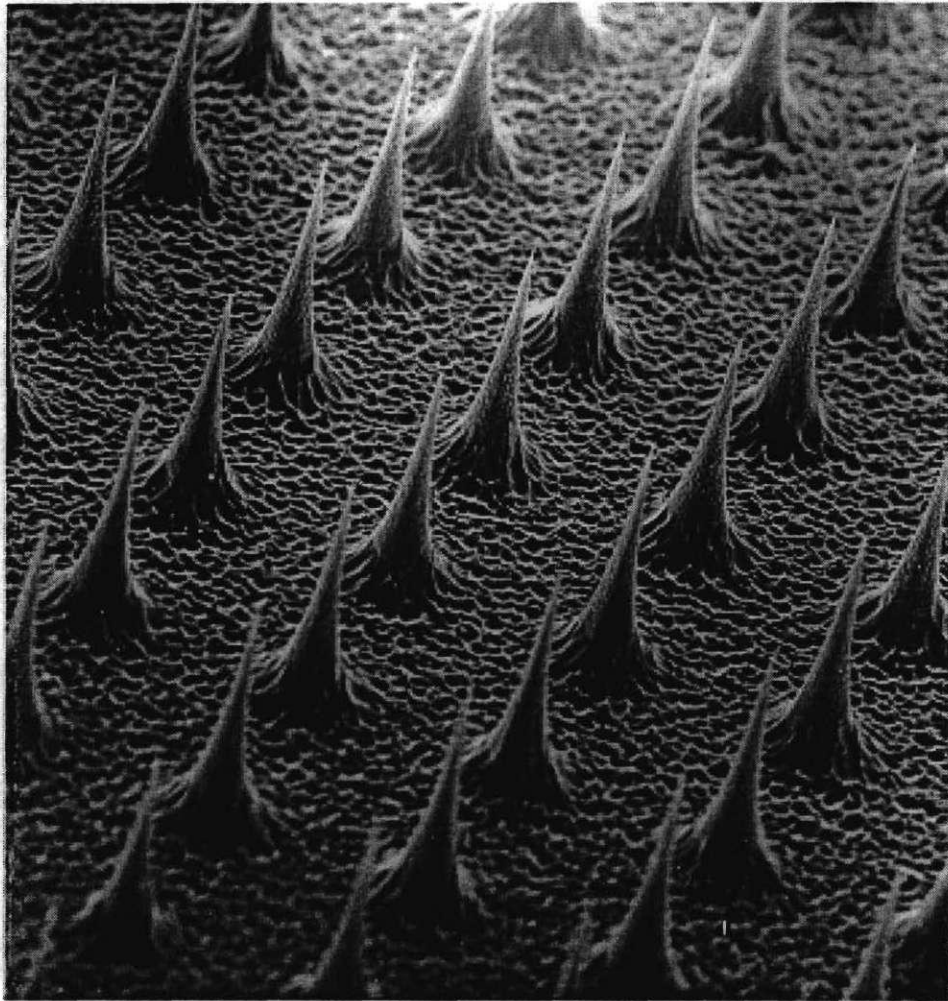
- - - - - - - - - - - - - - - - ~230 μm

Figure 16: Scanning Electron Micrograph Of Spikes.

Spikes' height: ~ 180 μm *Pressure: 150 mT*

Aspect Ratio: ~2.5 *Power: 180 W*
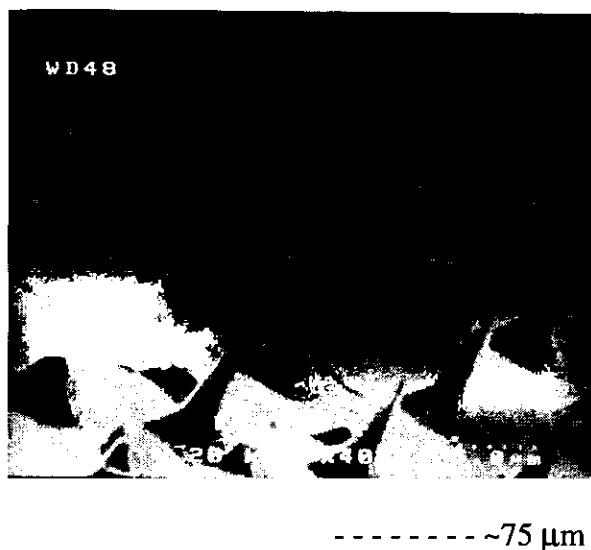
SF₆/O₂ ratio: 1.33 *Running time: 250 min*

Loading: two 2-inch wafers *Masks' diameter: 80 μm*

42

CHAPTER V

SKIN

Experiments on skin were designed to assess the mechanical and drug delivery properties of microspikes. First, the mechanical strength of microspikes was tested by experiments in which microspikes were inserted into and removed from skin. Second, the capacity of microspikes to enhance transdermal drug delivery was investigated: dye molecules, playing the role of drugs, were used to assess transport.

Materials and Methods

Experimental Setups and Protocols

The skin we used in our experiments was human skin collected in hospitals after autopsies and plastic surgery. The skin was kept in our laboratory in a freezer at -80°C. Prior to all experiments, one or several pieces of skin were removed from the freezer and allowed to thaw at room temperature. Either full-thickness skin or only the epidermis (stratum corneum + viable epidermis) was utilized. When only the epidermis was needed, a precise protocol was followed in order to detach the epidermis from the dermis:

1) The skin was allowed to thaw.

2) The fat, if any, attached to the dermis side of the skin was scraped off using the blunt handle of a scalpel (without a blade).

43

3) The skin was soaked in deionized water at 60°C for 2 minutes.

4) The wet skin was placed, dermis side down, on a piece of lab bench paper, absorbant side up, so that the wet dermis stuck to the lab bench paper.

5) The skin was stretched using tweezers and, in the meantime, the epidermis was peeled off using a spatula. During the peeling, the epidermis would fold over itself.

6) Once removed from the dermis, the epidermis was placed in a bath of deionized water and allowed to unfold. The stratum corneum side of the epidermis was oriented upwards (the stratum corneum was easily recognized because of its hydrophobicity).

7) The epidermis was checked for holes (water drops formed on surface of stratum corneum when it had holes). Pieces that contained holes were discarded.

8) The hole-free epidermis (stratum corneum facing up) was spread onto the waxy side of lab bench paper (to prevent the epidermis from folding back once taken out of the water).

9) The epidermis and the underlying lab bench paper were removed from the water bath and then cut into circles using a hole puncher for subsequent transport experiments.

10) The circles of epidermis (each attached to a circle of lab bench paper) that were not needed immediately for experiments were stored in a humid jar that was kept in a refrigerator.

To test the ability of microspikes to deliver a drug across skin, Franz transport chambers (FDC-100 # 20; Crown Glass Co. Inc., Somerville, NJ, USA) were used (Figure 17).
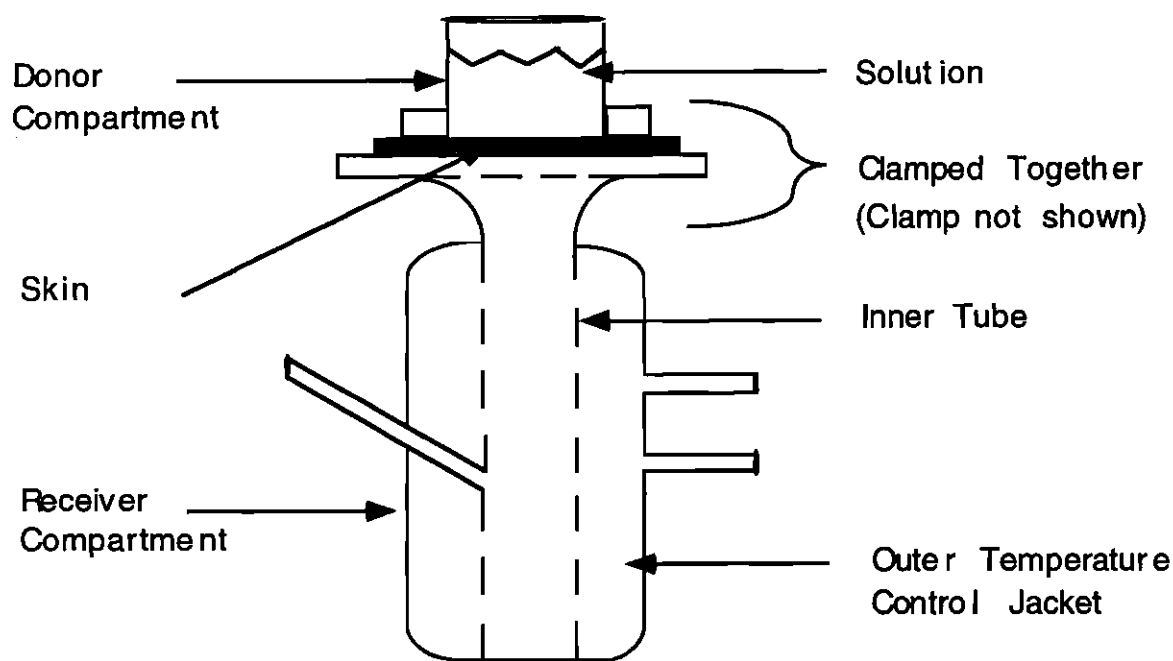
Figure 17 (not to scale): Franz Transport Chamber Used To Test The Ability Of Microspikes To Deliver Molecules Across Skin.

In such transport chambers, a piece of skin is sandwiched between a donor compartment and a receiver compartment. The donor compartment is a hollow cylinder (neither of the ends are closed). The receiver compartment consists of a hollow inner tube (only the bottom end is closed) surrounded by a temperature control jacket.

To test the permeability of the skin, the donor compartment is filled with an appropriate solution (e.g., a fluorescent dye). If the skin is not permeable, the solutes cannot cross into the receiver compartment. If the skin is permeable or rendered permeable, the solutes can diffuse through the skin and are collected in the receiver compartment of the transport chamber.

Two different protocols were followed depending on whether the transport experiments were qualitative or quantitative:

Qualitative Experiments

Qualitative experiments were performed in an attempt to obtain a rough estimate of the level of transport generated by microspikes. In these experiments, the donor compartment of transport chambers was filled with a blue dye. Transport was assessed by looking, with the naked eye, at the staining (if any) of the solution in the receiver compartment and of the skin sample.

1) A circle of epidermis was placed in a deionized water bath and separated from its underlying lab bench paper.

2) The circle of epidermis was once more checked for holes (water drops formed on surface of stratum corneum when it had holes).

3) The hole-free epidermis (stratum corneum facing up) was spread onto a cushion (human dermis, foam or latex) and removed from the water bath; the cushion's role was to ease the piercing of the epidermis in the subsequent step and to simulate the dermis found *in vivo* below the epidermis.

4) A device (an array of microspikes) was positioned in the middle of the epidermis circle in such a way that the spikes (sharp tips down) were resting on the stratum corneum.

5) A 2-mm-diameter wooden stick was used to apply pressure on the device in order to force the microspikes into the epidermis.

6) The epidermis (with the microspikes embedded in it) was separated from its cushion in a deionized water bath and was spread (stratum corneum down) on the waxy side of a piece of lab bench paper for subsequent microscope inspection.

7) The epidermis was inspected under a microscope to verify that the microspikes actually pierced the epidermis all the way through; the epidermis was also checked for possible tears (other than the microspike holes) due to mishandling.

8) If the epidermis showed tears not caused by microspikes, it was discarded; if the epidermis was tear free but was not pierced all the way through by the microspikes, steps 3 through 7 were repeated.

9) The pierced and tear-free epidermis (stratum corneum up) was placed on a piece of screen (house window screen with a 2 mm by 1.5 mm mesh; Home Depot, Atlanta, GA, USA) and then mounted in a transport chamber between the donor and receiver compartments. Prior to mounting the epidermis, the receiver compartment was filled with saline (phosphate-buffered solution: 0.01 M phosphate buffer, 0.0027 M potassium chloride, and 0.137 M sodium chloride, pH 7 at 25^0C; Sigma Chemical Co., St. Louis, MO, USA). The role of the screen was to support the epidermis and prevent it from buckling towards the receiver compartment of the transport chamber. Vacuum grease (Dow Corning high vacuum grease; Dow Corning Corporation, Midland, MI, USA) and a mechanical clamp were used in order to provide a good seal between the edges of both compartments (Figure 18). The seal ensured that if transport occurred later in the experiment it could only be due to the permeability of the epidermis, not due to a leak.

10) The donor compartment was filled half-way with saline. After a couple of minutes, Trypan Blue dye ($C_{34}H_{28}N_6O_{14}S_4$, MW = 960.82 g/mol; Sigma Chemical Co., St. Louis, MO, USA) was added until the donor compartment was entirely full.

11) Transport was assessed when blue dye was seen (with the naked eye) in the receiver compartment. A magnet lying at the bottom of the receiver compartment was used to stir the saline in order to enhance the blue dye's mixing throughout the receiver compartment in case of transport.

Device
(Spikes' Array)

Blue Dye
+ Saline

Clamped Together

Screen

Saline

Line Indicating Level
of Saline in Receiver
Compartment

Magnet (Stirrer)

Figure 18 (not to scale): Experimental Setup For Transport Experiments; The Temperature Control Jacket Was Not Used.

Quantitative Experiments

Quantitative experiments were run to quantify transport enhanced by microspikes. Similar to the qualitative experiments, a fluorescent dye was used to assess transport; however, the detection method, in these quantitative experiments, was much more sensitive because fluorescence detected by a spectrofluorimeter rather than absorbance detected by the human eye was used.

1) A circle (2.5 cm in diameter) of epidermis was placed in a deionized water bath and separated from its underlying lab bench paper.

2) The circle of epidermis was once more checked for holes.

3) The tear-free epidermis (stratum corneum up) was placed on a piece of screen and then mounted in a transport chamber between the donor and receiver compartments. Prior to mounting the epidermis, the receiver compartment was filled with saline. Vacuum grease and a mechanical clamp were used for the same reasons as in the "qualitative protocol".

4) A device (array of microspikes) was positioned in the middle of the epidermis mounted in the transport chamber in such a way that the microspikes (sharp tips down) were resting on the stratum corneum.

5) A 2-mm-diameter wooden stick was used to apply pressure on the device in order to force the microspikes into the epidermis.

6) The donor compartment was filled with 10^{-3} M calcein ($C_{30}H_{26}N_2O_{13}$, MW = 623 g/mol; Sigma Chemical Co., St. Louis, MO, USA).

7) To fully characterize transport across the epidermis, changes in the experimental setup were brought in certain experiments; in some cases a voltage was applied across the epidermis during defined periods by means of Ag/AgCl electrodes (E242; In Vivo Metrics, Healdsburg, CA, USA) connected to a DC power supply (HPE 3620A; Hewlett Packard, Loveland, CO, USA): one electrode was placed in the donor compartment of the transport chamber whereas the other electrode was inserted into the receiver compartment. Also, the device embedded in the epidermis was sometimes removed after a certain amount of time to measure transport across the epidermis with and without the array.

8) Transport was quantified after the experiments by measuring the concentration of calcein in the receiver compartment of the transport chamber by means of spectrofluorimetry. A magnet lying at the bottom of the receiver compartment was used to stir the saline in order to enhance the calcein's mixing throughout the receiver compartment in case of transport.
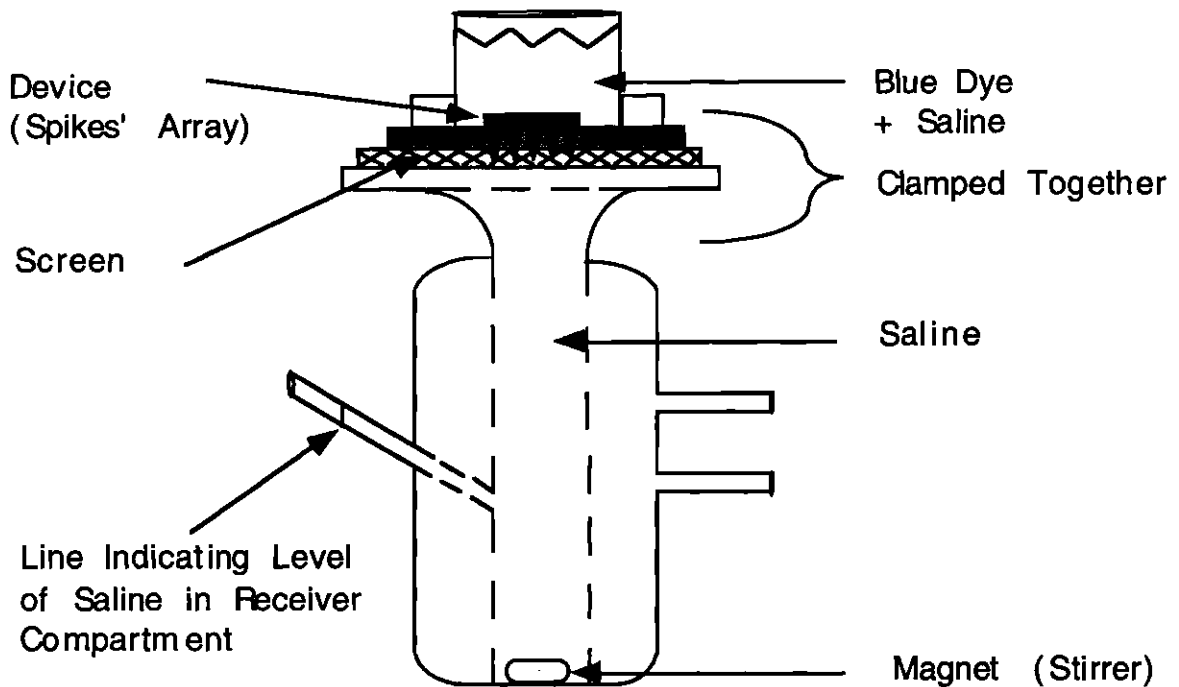
Spectrofluorimetry

Spectrofluorimetry is a very sensitive technique that enables detection of very low concentrations of a given fluorescent dye, calcein in our experiments. A sample with an unknown concentration of calcein is loaded into the spectrofluorimeter (QM-1 fluoresence spectrometer, Photon Technology International, Ontario, Canada). A beam of blue light shining through a 2-nm-bandpass slit at a wavelength of 488 nm is used to excite the sample. As a result of this excitation, emission light from calcein is scattered from the sample. Only the emission light scattered from the sample at a 90^0 angle with respect to the excitation light beam is collected through a 4-nm-bandpass slit. This emission light is digitally converted into a number of counts per seconds (or photons per seconds).

It is known that when calcein is excited with a 488-nm light, most of the resulting emission light has a wavelength of ~515 nm (U.F. Pliquett *et al.*, 1996). Therefore, if this emission light is converted into a number of counts per second and plotted as a function of wavelength, a curve exhibiting a peak at ~515 nm will appear provided that the calcein concentration in the sample is within the detection range of the spectrofluorimeter. The integration of the curve yields a number of counts per second corresponding to the total area under the curve: this total area can be converted into a concentration by means of a calibration curve. To make a calibration curve, samples with known concentrations of calcein are analyzed in the spectrofluorimeter. For each of the samples, a total area is determined. The calibration curve is obtained by plotting the total areas versus the different corresponding concentrations; the relationship on a log/log scale should be linear with a slope of 1.

In our experiments, the total areas of the emission spectra were determined from 505 nm to 535 nm with a 5-nm increment (1 second per point). Because we used calcein diluted in PBS, we subtracted the background signal equal to the total area of the PBS spectrum from the total areas of the emission spectra measured during our experiments.

Assessment of Transport Across Epidermis

During our experiments, samples were taken from the receiver compartment of transport chambers and measured by spectrofluorimetry. Using a calibration curve, the fluorescence measurements were converted into calcein concentrations. Then, these calcein concentrations were converted into fluxes (across epidermis) using the following formula:

$$F = \frac{CW_tV}{AT}$$

where:

F=flux (g/cm^{2}h)

C=calcein concentration in receiver compartment (mol/l)

W$_t$=molecular weight (623 g/mol)

V=volume of receiver compartment (5.3×10^{-3} l)

A=area of skin (0.79 cm^2)

T=time between samples (h)

Results

Mechanical Properties of Spikes

The mechanical properties of microspikes were tested on skin. We placed 16 by 16 arrays of microspikes made with 50-μm masks (~140-μm-tall microspikes) onto pre-cut pieces of skin (stratum corneum up) and pressed them against the skin using a thin wooden stick (2 mm in diameter). Under a microscope, we looked for possible piercing of the

51

stratum corneum by the microspikes. Because skin is so thick (a few mm), compared to our devices (~140 μm), and so highly deformable, it would fold around the devices making it very difficult to assess skin penetration.

Although these experiments did not allow us to determine whether microspikes could pierce stratum corneum, they showed us that microspikes had good mechanical properties; indeed, SEM inspection of the microspikes after the experiments revealed that, within an array, 95% of the microspikes remained intact while the others broke only at the tip (top 5-10 μm). Considering the fact that a large force, ~20 N (the force was calculated by converting the load applied to the microspikes into kg and multiplying it by the gravitational constant, 9.81 m/s^2), compared to the size of the devices, was applied to the microspikes, these first results were considered very promising. However, we still did not know whether microspikes could penetrate skin.

Realizing that a much thinner skin would facilitate the assessment of skin penetration, we decided to work with epidermis only; this meant working with a thickness of at most 200 μm instead of several mm.

As previously mentioned, one of the goals of this research is to pierce stratum corneum, a sublayer of epidermis. Therefore, we could have worked with stratum corneum only instead of with epidermis. However, stratum corneum alone is very fragile and is difficult to handle because it is so thin. Also, we assumed that epidermis would be thin enough to allow us to see penetration if it occurred. This is the reason why we chose epidermis over stratum corneum.

Following the above-mentioned protocol, epidermis was stripped off. As in the experiments with full thickness skin, 16 by 16 arrays of ~140-μm-tall microspikes were pressed against epidermis. In order to eliminate any bias that could have been created by the

removal of the dermis layer, the epidermis, after being stripped off, had been placed back onto the dermis. Using a microscope, we saw that more than 95% of the microspikes within an array had pierced not only stratum corneum but the entire epidermis. Moreover the microspikes that penetrated the epidermis remained mostly intact; less than 5% of the spikes' tips (the top 5-10 μm) broke during the epidermis penetration. 20 by 20 arrays of microspikes made with 80-μm masks (~180-μm-tall microspikes) were also pressed against epidermis. Inspection under a microscope revealed that all the microspikes pierced epidermis and that less than 5% broke (Figure 19 a/b).

Smaller spikes that would pierce stratum corneum without crossing the full epidermis can be made easily, but were not examined in this study.
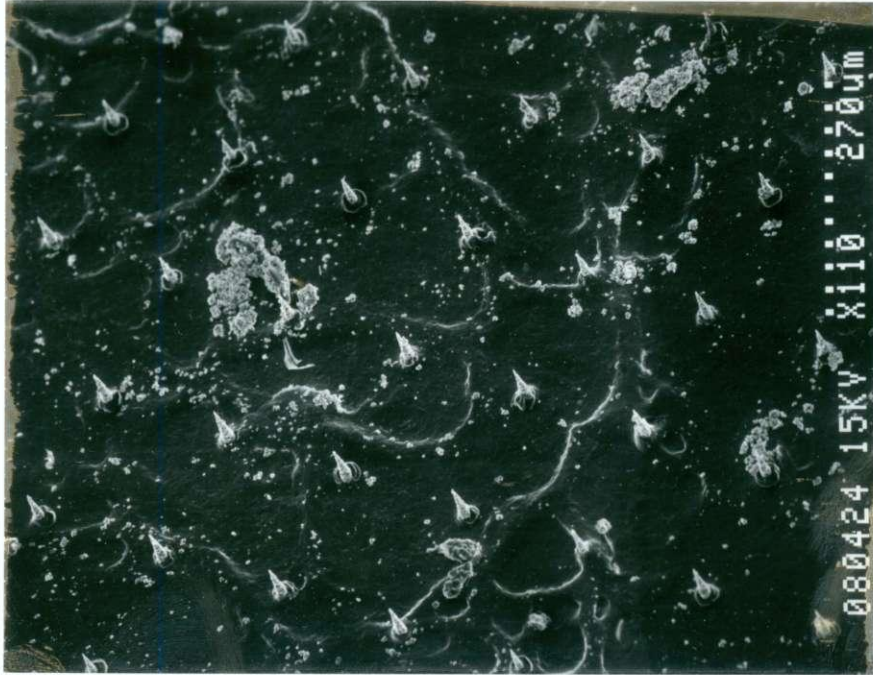
Figure 19: Scanning Electron Micrograph Of Epidermis Pierced By 180-μm-Tall Microspikes

a) magnification: 110 X.
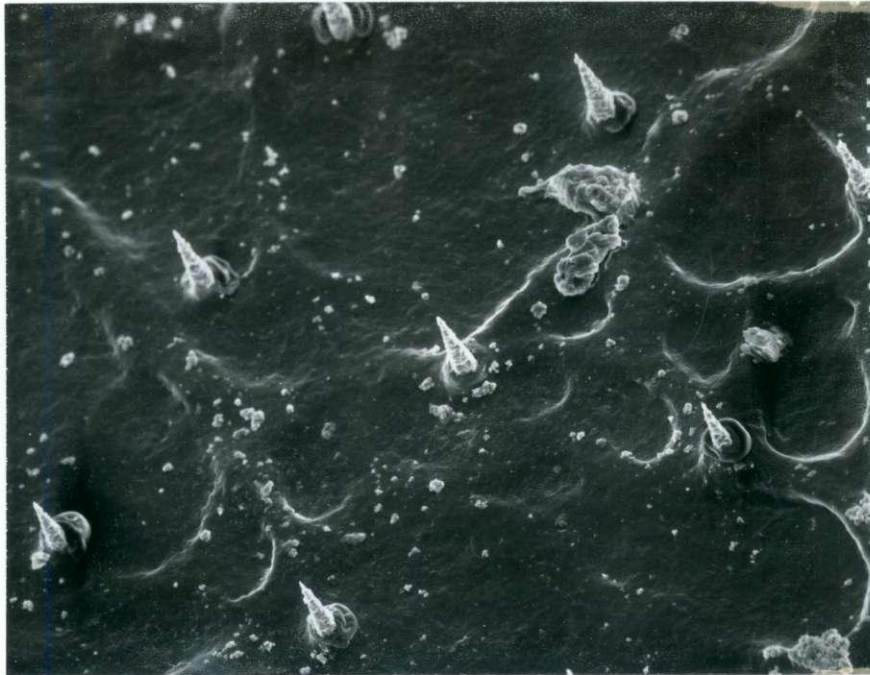
Figure 19: Scanning Electron Micrograph Of Epidermis Pierced By 180-μm-Tall
Microspikes

b) magnification: 250X

This experiment, which was successfully repeated more than ten times, showed that the microspikes were sturdy enough to pierce epidermis all the way through and that little force (as low as ~6 N for ~140-μm-tall spikes and as low as 3 N for ~180-μm-tall microspikes) was required to achieve piercing. For comparison purposes, a 6-N force is approximately equivalent to the force required to push a button in an elevator.

This was a significant finding in our research since, before this experiment, we did not know whether such small structures as our spikes could be strong enough to penetrate skin. Following these results, we started investigating the transport of molecules across skin.

Qualitative Transport Experiments

The above-mentioned protocol was followed during the transport experiments. A blue dye was used for easy detection (with the naked eye) of transport across epidermis. This coarse detection method was chosen because we were first interested in seeing a big effect; namely, we wanted to find out whether our devices could yield significant transport across skin.

The fact that we were using epidermis instead of full-thickness skin was not an issue since studies showed that stratum corneum is the main barrier in transdermal transport of molecules (Fartasch, 1996); once molecules are chemically, physically, or electrically transported across stratum corneum, they diffuse easily through deeper epidermis and dermis. Also, working with epidermis is a standard technique in literature in the case of drug delivery studies.

Control experiments were first performed; in these experiments, run for 24 hours, the epidermis had not been pierced. At the end of these experiments, the saline in the receiver

compartment of the transport chamber had not turned blue, attesting to a good seal between the compartments in the chamber and to the fact that skin had not been damaged during preparation.

As for the experiments involving arrays of spikes, they did not lead to transport of blue dye in amounts detectable with the naked eye. Therefore, we assumed that the devices might have been pressed too much against the epidermis, leaving insufficient space for the blue dye to flow between the arrays and the epidermis. This lack of space would have been responsible for yielding a limited transport.

In subsequent experiments, the devices were pressed into the skin and then carefully removed from the epidermis (still mounted in the transport chamber) using tweezers in an attempt to allow the blue dye to flow freely through the holes left by the spikes. After the removal of the spikes, these experiments were run for 24 hours. None of these experiments yielded transport detectable with the naked eye.

Based on the results of these experiments, we decided to bring a modification to the original experimental setup. All the steps of the qualitative transport experiments protocol were followed through step 9. Then, a wooden stick was glued to the backside of the array and the stick was forced to oscillate horizontally, enabling vibration of the array. The oscillation of the wooden stick was ensured by an oscillating device (mini shaker type 4810; Bruel & Kjoer, Copenhagen, Denmark) put in contact with the stick (Figure 20). The goal of this modification of the experimental setup was to enhance blue dye transport by, upon vibration of the array, creating more space between the array and the epidermis and by enlarging the holes made by the spikes. Once the stick was glued and the array was vibrating, the remaining steps of the protocol (steps 10 and 11) were completed.
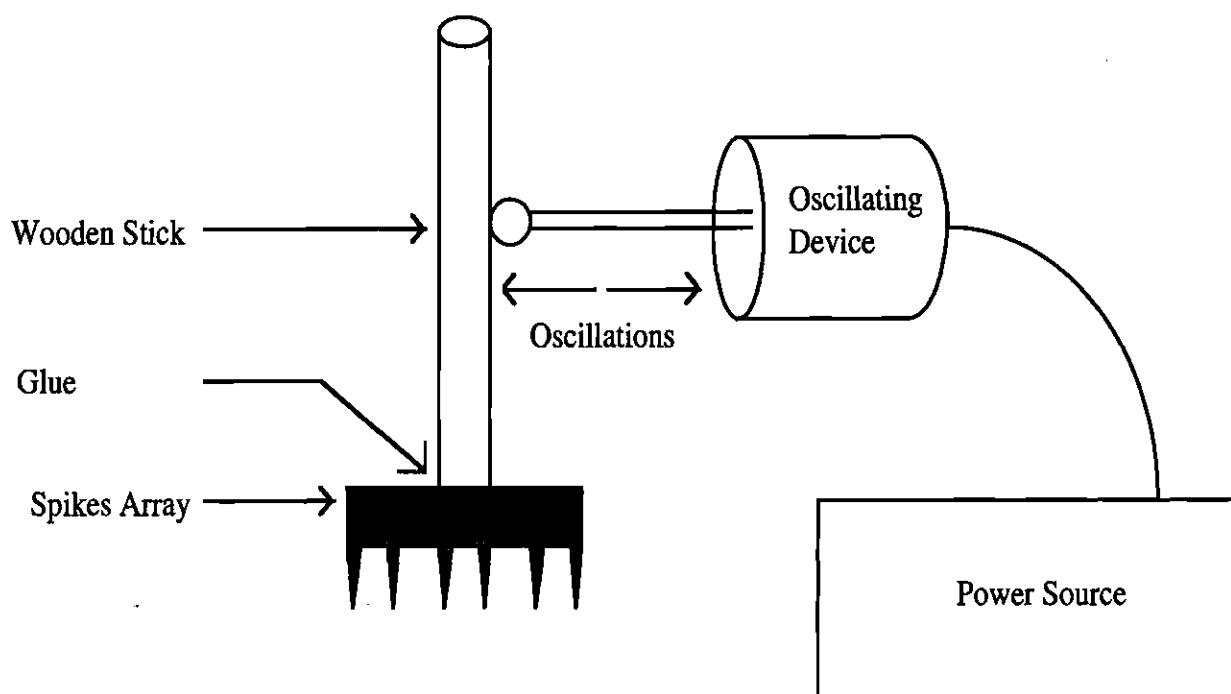
Figure 20 (not to scale): Vibration Of The spikes' Array Due To Oscillation Of The Wooden Stick (although not represented in this figure, the spikes are embedded in a piece of epidermis mounted in a transport chamber).

In these experiments involving vibration of the spikes' array, blue dye was added to the donor compartment of the transport chamber 5 minutes prior to turning on the oscillating device. The frequency and amplitude of the vibrations were set respectively at 10 Hz and ~6 mm. These experiments did not yield visible transport. However, after the experiments, the epidermis samples were removed from the transport chambers and inspected under a

microscope. Blue dots arranged in a pattern similar to that of the microspikes were observed on the side of the epidermis that had faced the receiver compartment during the experiments. It was not clear yet whether blue dye was just coloring the microspike holes on the stratum corneum side of the epidermis or if blue dye was going all the way through the epidermis, leading to transport across the epidermis at levels too low to be detectable with the naked eye.

In subsequent experiments, prior to applying vibration, an oblong tear (~40 μm by ~400 μm) was intentionally made in epidermis in the vicinity of the microspikes' array. The goal was to be able to compare the staining of a tear (through which transport would occur) with that of the microspike holes. As expected, significant amounts of blue dye were collected in the receiver compartment of the transport chamber presumably due to transport through the tear. After these experiments, on all the epidermis samples, an array of blue dots corresponding to the microspike holes and a tear whose edges were colored in blue were observed on the side of the epidermis that had faced the lower compartment; hence, we had confirmation that most of the transport that we saw was due to the tear and not to the holes made by the microspikes. It was noticed that the blue dye had spread around the tear; also, at the very edge of the tear, the blue was very dark. As for the microspike holes, they were stained in a way similar to that of the tear. Figure 21 shows the staining of microspike holes and of a tear on a piece of epidermis at three different magnifications. A similar staining was also observed when microspikes were inserted into epidermis and later removed (without being vibrated); however, the spread of blue dye around the microspike holes was not as large as when microspikes were vibrated. This suggested that when blue dye flows through epidermis, as it did in the case of the tear, it leaves dark stains on the side of epidermis facing the receiver compartment.

These observations were very valuable because they allowed us to realize that transport occurred through the microspike holes but in amounts not detectable with the naked eye. Therefore we decided to use a much more sensitive detection method that would allow us to quantify low levels of transport not visible with the naked eye.
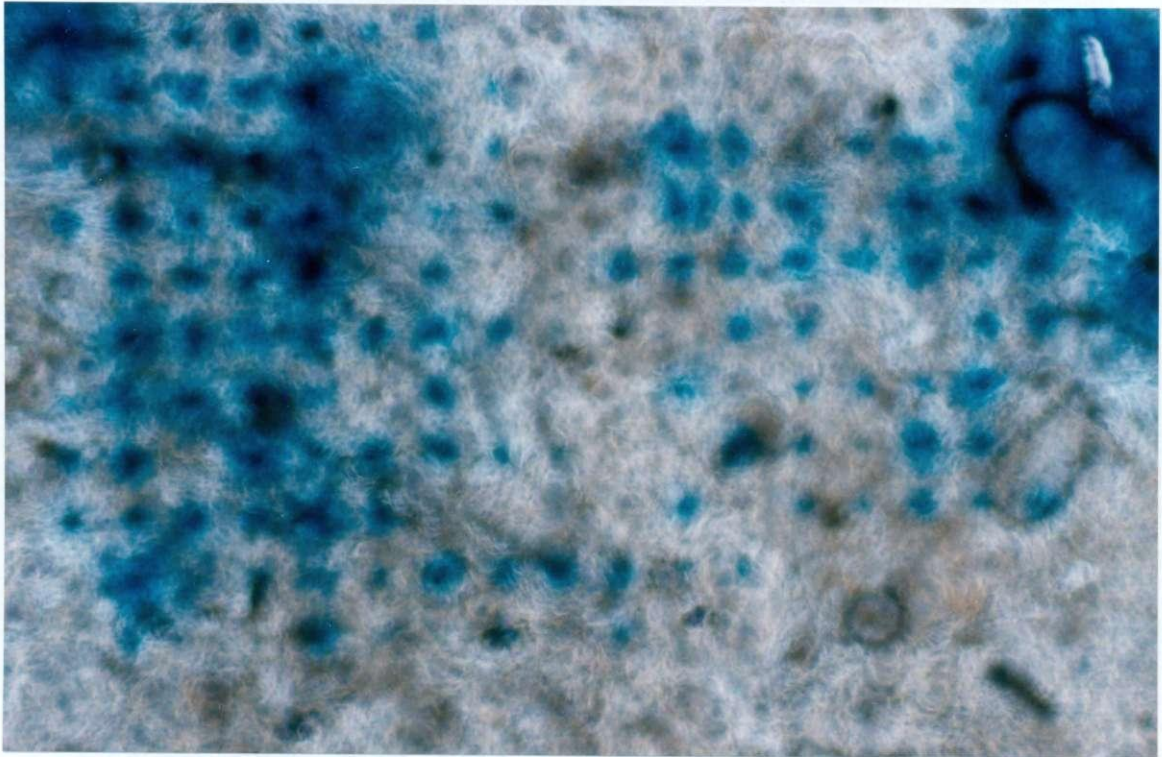
Figure 21: View Of Epidermis (side facing lower compartment of transport chamber)

a) Array Of Spike Holes Dyed In Blue; The Tear Is Visible In The Right Upper Corner (magnification: 40 X).
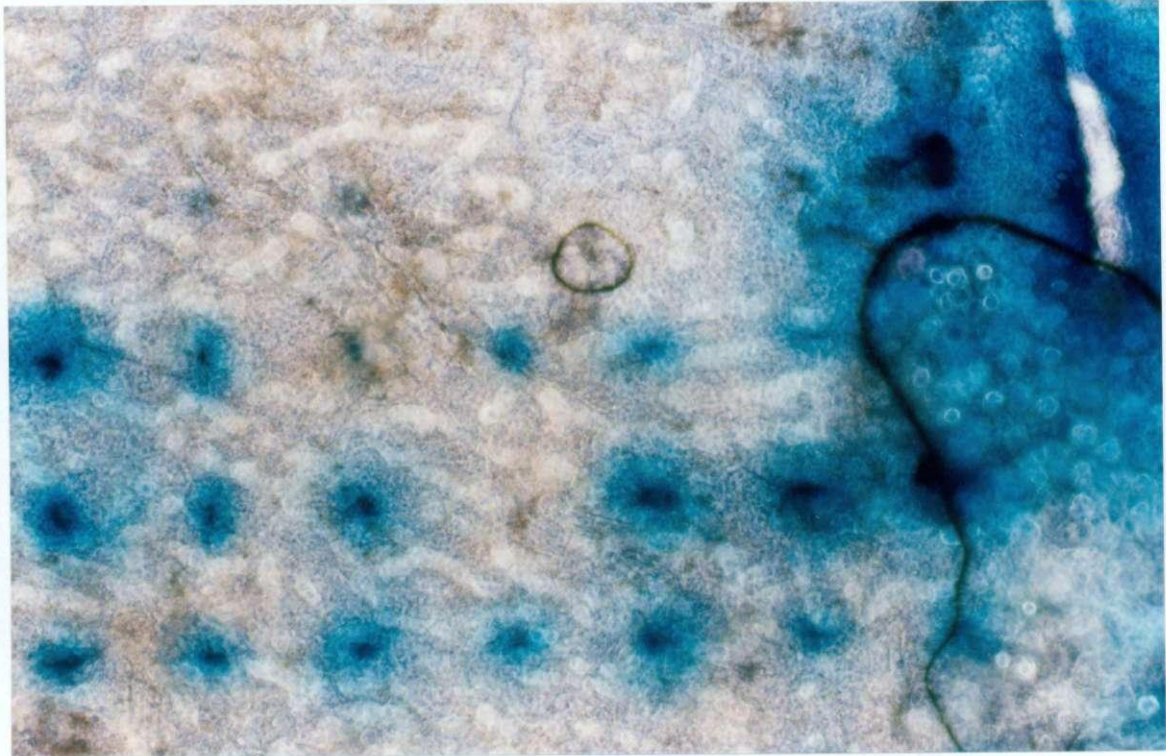
b) Spike Holes And Tear (right upper corner); Dark Blue Can Be Seen On The Edges Of The Tear And In The Center Of The Blue Dots Encircling The Spike Holes (magnification: 100 X).
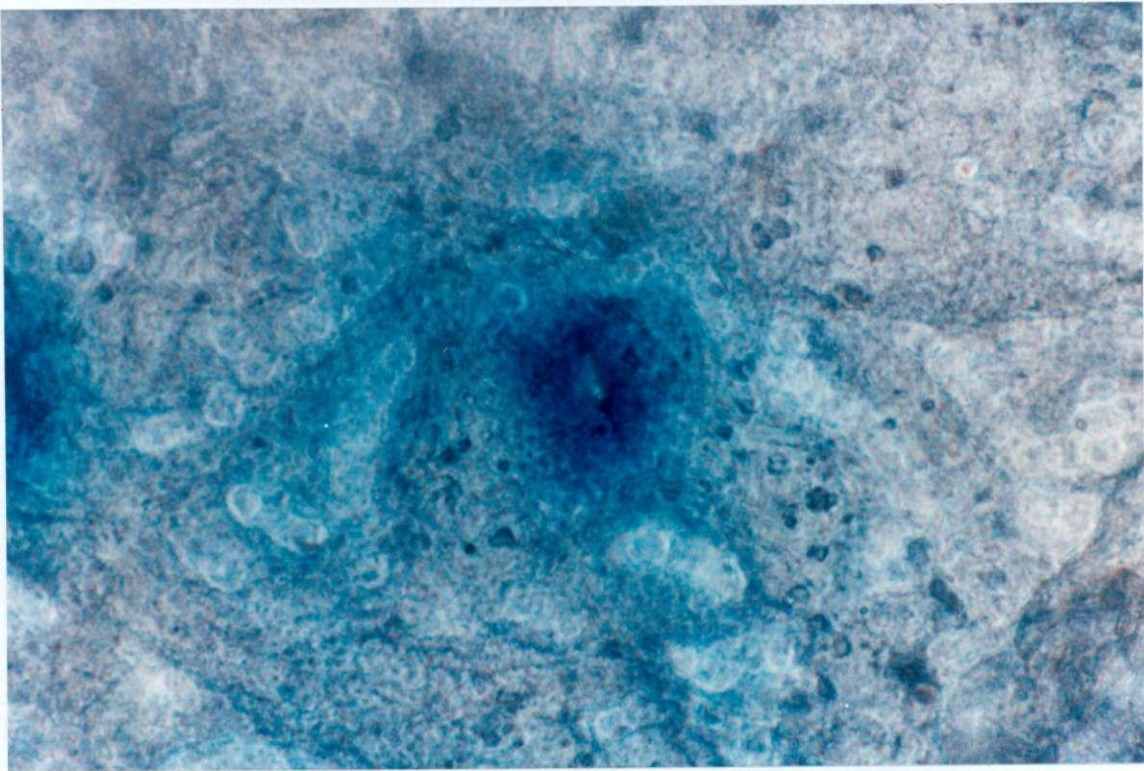
c) Hole Made By A Spike; The Hole Was Stretched Vertically Due To Oscillation. Dark Blue Dye Is Clearly Visible Around The Hole (magnification: 400 X).

Quantitative Transport Experiments

The goal of these experiments was to quantify the transport of molecules induced by microspikes across epidermis. A fluorescent dye, calcein, was used to characterize transport. The donor compartment of transport chambers was filled with calcein prior to running experiments. Concentrations of calcein in the receiver compartment were determined at regular time intervals during the experiments by means of spectrofluorimetry.

To ease the detection of calcein transport, microspikes larger than those used in the qualitative experiments were fabricated; our rationale was that larger spikes would yield more transport. 20 by 20 arrays of ~180-μm-tall microspikes were made with 80-μm masks.

The epidermis and the transport chambers were prepared according to the above-mentioned protocols. The passive diffusion of calcein across epidermis was first investigated. A piece of epidermis was mounted onto a transport chamber and the donor compartment was filled with calcein (10^{-3}M). Samples from the receiver compartment were taken every 60 minutes. Results showed passive fluxes of calcein across epidermis of ~4.2×10^{-3} μg/cm^{2}h. Then, the effect of microspikes on transport was measured. Passive diffusion was first initiated; after an hour, a sample was taken from the receiver compartment and the flux of calcein across epidermis was calculated. If the flux was greater than 4×10^{-3} μg/cm^{2}h, the piece of epidermis was replaced and the experiment restarted. If the flux was lower than 4×10^{-3} μg/cm^{2}h, the microspikes were inserted into the epidermis and the flux of calcein across epidermis was measured over a one-hour period. Then, the microspikes were removed and transport was allowed for one more hour. Results showed that, while the microspikes are embedded in epidermis, the transport of calcein across epidermis is as low as in the case of passive diffusion: they provide no transport enhancement (Figure 22). However, upon removal of the microspikes, transport of calcein is enhanced; this yielded fluxes of calcein of ~5.6×10^{-1} μg/cm^{2}h, which approximately represents a 130-fold increase in flux compared to passive diffusion (Figure 22).
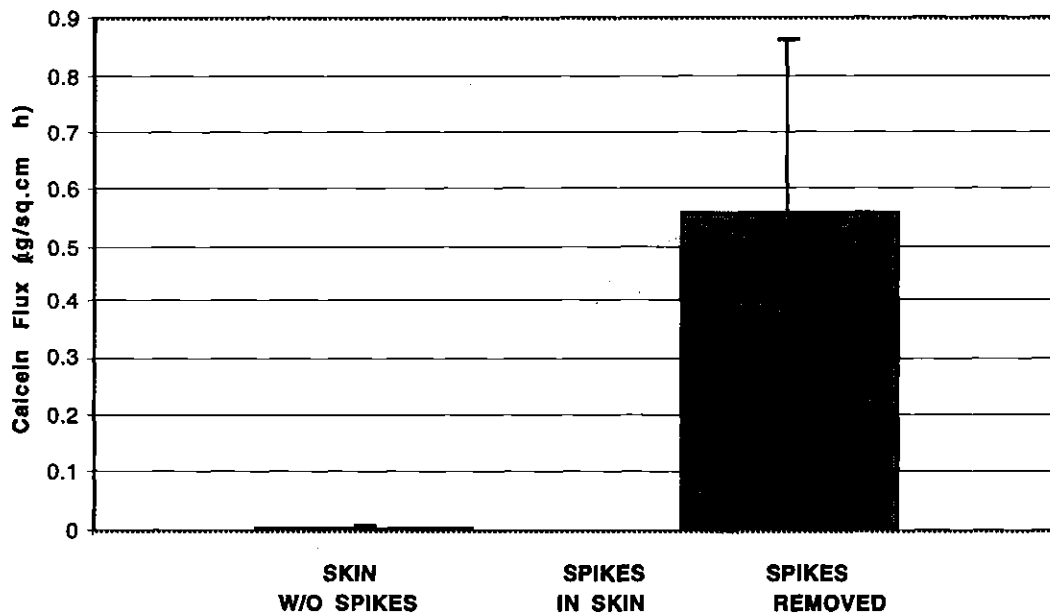
Figure 22: Calcein Fluxes (Average Values, Standard Deviation Bars Are Shown) Obtained In The Following Conditions:

- SKIN W/O SPIKES=Unpierced epidermis

-SPIKES IN SKIN=Microspikes embedded in epidermis

-SPIKES REMOVED=Microspikes inserted in epidermis then removed

Passive diffusion was first measured across the whole epidermis sample (0.79 cm². When spikes were inserted into epidermis, the calcein flux F_1 was calculated across the area covered by microspikes' array (a 20 by 20 microspike array, microspikes' base diameter of 80 μm, and microspike-to-microspike spacing of 75 μm resulting in an array area of 0.0915 cm²). The array area was subtracted from the epidermis area (0.79-0.0915 = 0.6985 cm²); the passive diffusion flux calculated across this new area (0.6985 cm²) was

subtracted from F₁ to yield the "SPIKES IN SKIN" flux. The same approach was followed to calculate the "SPIKES REMOVED" flux.

It is known that transdermal transport of calcein is enhanced by low voltages (Prausnitz *et al.*, 1996). For comparison purposes, we ran experiments in which a voltage was applied (a 2V-voltage was applied but some of it was most likely across the electrodes and the electrode-electrolyte interface) across epidermis by means of two Ag/AgCl electrodes (one in the donor compartment and one in the receiver compartment) connected to a DC power supply. Since calcein has a negative overall charge, the donor-compartment electrode was connected to the negative output of the power supply whereas the receiver-compartment electrode was connected to the positive output of the power supply. In these conditions, we measured a flux of $\sim 1.8 \times 10^{-2}$ μg/cm²h (Figure 23). This revealed that the transport of calcein across epidermis enhanced by microspikes is greater by a factor of 30 (when the microspikes are inserted and later removed from epidermis) than the transport generated by a 2V-voltage. This confirmed the great potential of microspikes as transdermal drug delivery devices.

The combination of microspikes with voltage proved to enhance even more transport. Microspikes were inserted into epidermis and 2V were applied simultaneously. An hour later, the microspikes were removed but the voltage was applied for another hour. The voltage coupled with inserted microspikes yielded fluxes of $\sim 3.4 \times 10^{-1}$ μg/cm²h (Figure 23). Removing the microspikes but maintaining the voltage enhanced the transport of calcein by approximately a factor of 40: fluxes of ~ 14.4 μg/cm²h were obtained (Figure 23).

Finally, we investigated the effect of horizontal and vertical vibrations of microspikes on the transport of calcein across epidermis. The setups were similar to the one used for the qualitative experiments. Horizontal vibrations of microspikes embedded in epidermis yielded a flux of calcein across epidermis of ~2.2 μg/cm^{2}h (Figure 24). When the vibrations were stopped and the microspikes removed from the epidermis, the transport of calcein only decreased to ~1 μg/cm^{2}h (Figure 24). As for vertical vibrations of microspikes, a calcein flux of ~7.8×10^{-1} μg/cm^{2}h was achieved (Figure 24). Upon removal of the microspikes from epidermis, the flux decreased to ~5×10^{-1} μg/cm^{2}h (Figure 24).

The use of horizontal vibrations led to more transport than when microspikes were inserted into epidermis and later removed but they did not allow to reach the levels of transport obtained when voltage was coupled with microspikes. As for vertical vibrations, they yielded a calcein flux a little smaller than the one attained when microspikes were inserted into epidermis and later removed. This is probably due to the fact that horizontal vibrations enlarge microspike holes whereas vertical vibrations may not.

These quantitative transport results show that when microspikes are embedded in epidermis and left there, they do not enhance transport of calcein, at least not in a significant way. However, when microspikes are inserted into epidermis and then removed, the calcein transport is increased by more than two orders of magnitude compared to passive diffusion. This suggests that when microspikes are embedded into epidermis, they may create transport pathways, but block them so as to prevent meaningfully increased calcein transport; nevertheless the enhancement of transport by application of a voltage across epidermis in conjunction with microspikes suggests that when microspikes are embedded into epidermis, they create pathways for calcein; calcein molecules cannot diffuse through these channels unless an extra driving force, such as a

66

voltage drop across epidermis, is applied. When microspikes are inserted into epidermis and then removed, they leave channels in epidermis that are large enough to increase transport of calcein by a factor of 130 compared to passive diffusion; this enhancement is even greater when a voltage is applied simultaneously: for a voltage of 2V, calcein transport is increased by a factor of 3600. Vibrating inserted microspikes led also to enhanced transport: a 200-fold increase and a 530-fold increase, compared to passive diffusion, were observed for vertical and horizontal vibrations respectively.
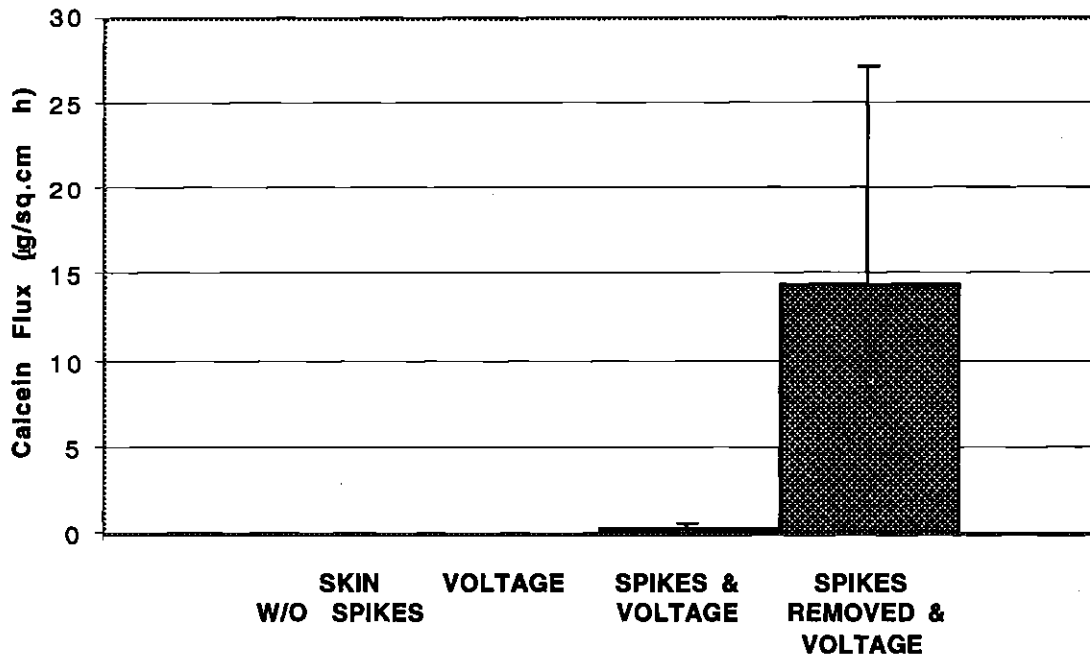
Figure 23: Calcein Fluxes (Average Values, Standard Deviation Bars Are Shown) Obtained

In The Following Conditions:

- SKIN W/O SPIKES=Unpierced epidermis

-VOLTAGE=Voltage across epidermis (only one data point collected)

-SPIKES & VOLTAGE=Microspikes embedded in epidermis + 2V voltage

-SPIKES REMOVED & VOLTAGE= Microspikes inserted then removed + 2V voltage

When the microspikes were removed (after being inserted into the epidermis) and a voltage was applied, the flux of calcein (F_2) was calculated across the array area. The "SPIKES & VOLTAGE" flux was calculated across the whole epidermis area (including the area covered by the array) and subtracted from F_2 to yield the "SPIKES REMOVED & VOLTAGE" flux.

2.5

2

1.5

Calcein Flux µg/sq.cm h)

1

0.5

0

SKIN   SPIKES &   SPIKES   SPIKES &   SPIKES
HOR. VIB.   REMOVED   VER. VIB   REMOVED
H. V.   V. V.
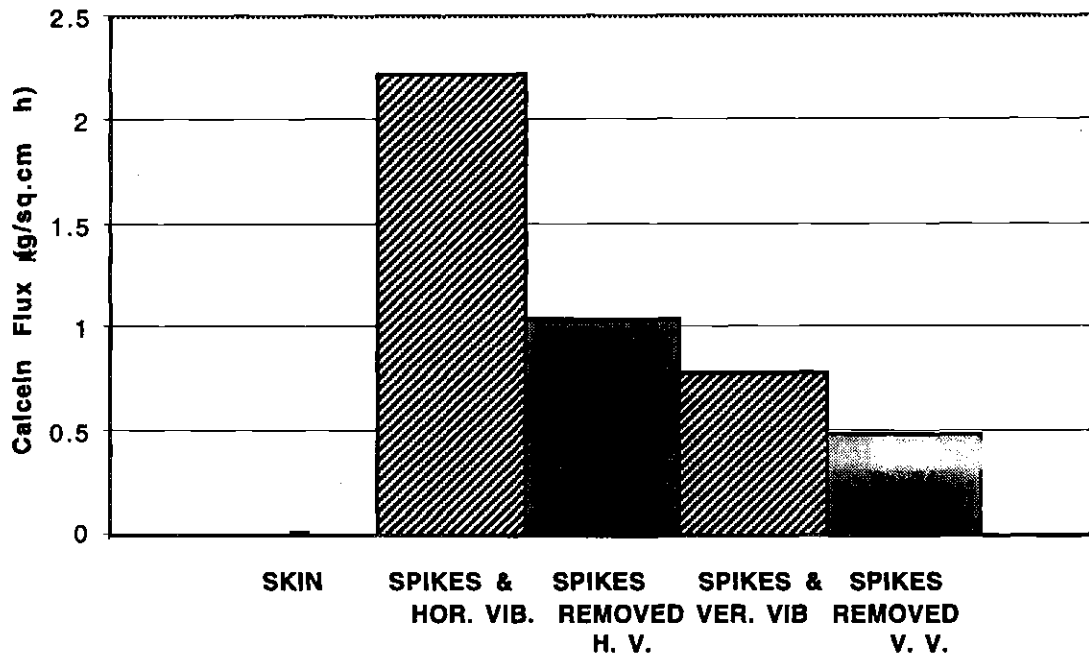
Figure 24: Calcein Fluxes (except for passive diffusion, only one data point was collected

for each experiment) Obtained In The Following Conditions:

- SKIN=Unpierced epidermis

-SPIKES & HOR. VIB.=Microspikes embedded in epidermis and vibrated horizontally

-SPIKES REMOVED H.V.= Microspikes removed from epidermis after horizontal

vibrations

-SPIKES & VER. VIB.=Microspikes embedded in epidermis and vibrated vertically

-SPIKES REMOVED V.V.= Microspikes removed from epidermis after vertical vibrations

Passive diffusion was first measured across the whole epidermis sample (0.79 cm²). When

spikes were inserted into epidermis and vibrated (vertically or horizontally), the calcein flux

(F_3) was calculated across the area covered by microspikes' array (0.0915 cm²). The array

69

area was subtracted from the epidermis area ($0.79-0.0915 = 0.6985$ cm^2); the passive diffusion flux calculated across this new area (0.6985 cm^2) was subtracted from F_3 to yield the "SPIKES & HOR. VIB." and "SPIKES & VER. VIB." fluxes. The same approach was followed to calculate the "SPIKES REMOVED H. V." and "SPIKES REMOVED V. V" fluxes.

CHAPTER VI

DISCUSSION

Microfabrication

The Black Silicon Method (Jansen *et al.*, 1995) was applied to fabricate microspikes. This technique relies on a plasma based on fluorine/oxygen chemistries to etch silicon microspikes shielded by chromium masks. Microspikes with different aspect ratios were created by changing the SF_6/O_2 ratio within the plasma. For a pressure of 150 mT and a power of 180 W, it was shown that the tallest and sharpest microspikes were obtained with an SF_6/O_2 ratio of 1.33. Using these parameters and 50-μm-chromium masks, 140-μm microspikes were made; 80-μm-chromium masks led to the fabrication of 180-μm microspikes.

The characteristics of the microspikes' arrays can be easily modified; the height and base of the microspikes can be increased or decreased by changing the size of the chromium masks and to a lesser extent the SF_6/O_2 ratio: the microspikes' profile can be rendered positive or negative by playing with the SF_6/O_2 ratio: the microspike-to-microspike spacing within an array can be varied by modifying the dot-to-dot spacing on the photolithography mask. This implies that microspikes that are sufficiently tall to cross stratum corneum without reaching the dermis and sufficiently thin to make holes in stratum

corneum of submicron dimension can be fabricated; thus, it appears that microspikes having dimensions which should make their use painless are feasible.

Skin Experiments

All the experiments on skin were performed with microspikes that were fabricated under the conditions yielding the largest aspect ratio.

To assess the mechanical properties of microspikes, 16 by 16 arrays of 140-μm microspikes were fabricated as well as 20 by 20 arrays of 180-μm microspikes. Arrays of 140-μm microspikes were pushed with a force of ~20N against full-thickness skin. Inspection under a light microscope revealed that the microspikes exhibited excellent mechanical properties. More than 95% of the microspikes remained intact while the rest broke at the tip only. It was also shown that microspikes have sufficient mechanical strength to cross epidermis; within an array of 140-μm microspikes, more than 95% of the microspikes penetrated epidermis all the way through. Among these microspikes, more than 95% remained intact after penetrating epidermis whereas, within an array of 180-μm microspikes, all the microspikes penetrated epidermis and less than 5% were damaged after penetration. These results show that silicon microspikes have excellent mechanical properties and that they can be used efficiently to pierce skin. Therefore, silicon microspikes seem to be suitable, from a mechanical strength perspective, for transdermal drug delivery; for safety reasons, 0% breaking will be required in the final version of the drug delivery device.

Qualitative transport experiments run in Franz transport chambers and with a blue dye used as a drug model were performed with arrays of 140-μm microspikes. Looking with the naked eye at the receiver compartment of the transport chambers, it was not possible to assess transport of blue dye across epidermis even when the microspikes underwent horizontal vibrations in an attempt to create more space between the arrays and epidermis and to enlarge the spike holes. However, it was noticed that epidermis was colored by the blue dye during the experiments in a way suggesting that transport occurred but at levels too low to be detectable with the naked eye.

Therefore, quantitative experiments involving spectrofluorimetry and 180-μm microspikes were performed to measure precisely calcein transport across epidermis. It was shown that calcein transport is not significantly enhanced when microspikes remain embedded in epidermis (Figure 25). However, when microspikes are inserted into epidermis and later removed, the calcein transport is enhanced by two orders of magnitude to reach fluxes of ~5.6×10^{-1} μg/cm^{2}h (Figure 25). This increase in flux upon removing the microspikes is most likely due to the fact that when microspikes are embedded into epidermis, they obstruct the pathways that they create during their insertion. When a 2V voltage was coupled with microspikes embedded in epidermis, calcein fluxes of ~3.4×10^{-1} μg/cm^{2}h were obtained (Figure 25). It is interesting to note that these fluxes exceed by an order of magnitude the calcein flux generated when a 2V voltage alone was applied across epidermis (without microspikes). This suggests that when microspikes are embedded into epidermis, they create pathways for calcein molecules; however, without a driving force other than the concentration gradient, calcein molecules do not flow through these pathways. When the microspikes are removed but the voltage maintained, the calcein

transport reaches fluxes of ~14.4 $\mu g/cm^2 h$ (Figure 25); when the microspikes are removed

from epidermis, the pathways are unobstructed; this added to the electric driving force
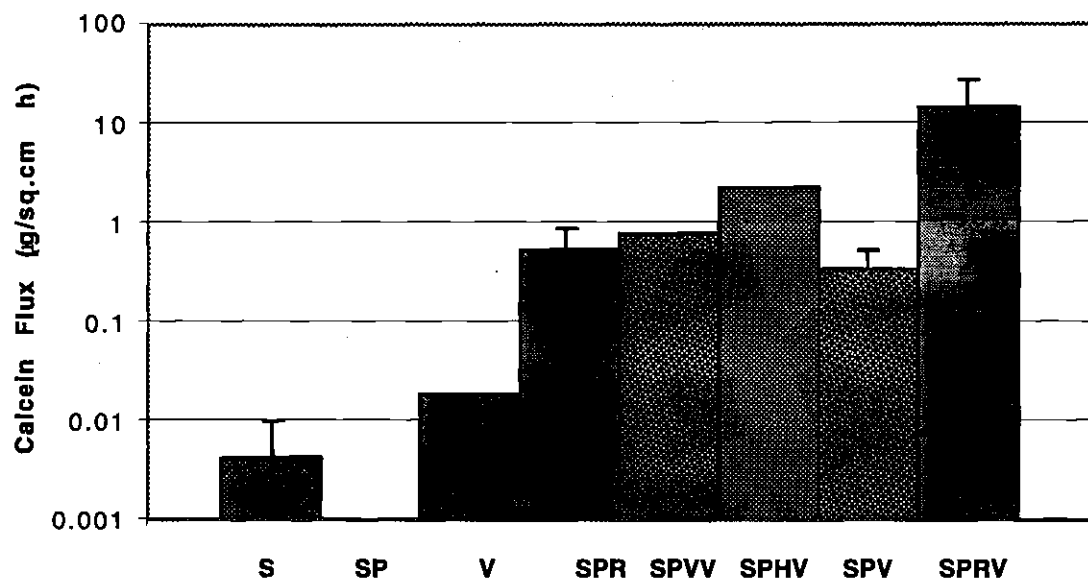
Figure 25: Calcein Fluxes Obtained In The Following Conditions:

- S= Unpierced epidermis

- SP=Microspikes embedded in epidermis

- V=Voltage across epidermis

- SPR=Microspikes inserted in epidermis then removed

- SPVV=Microspikes embedded in epidermis and vibrated vertically

- SPHV=Microspikes embedded in epidermis and vibrated horizontally

- SPV=Microspikes embedded in epidermis + 2V voltage

- SPRV=Microspikes inserted then removed + 2V voltage

results in a large calcein flux. This combination, spike holes and voltage yielded the largest calcein fluxes; it enhanced transport by 3 orders of magnitude compared to passive diffusion.

Horizontal and vertical vibrations of microspikes were also tried. Although vertical vibrations led to a calcein flux similar to those obtained when microspikes were inserted and removed, horizontal vibrations yielded a calcein flux of ~2.2 $\mu g/cm^2h$ (Figure 25), which represents a 530-fold increase over passive diffusion. In both horizontal and vertical cases, the removal of the microspikes led to a 50% decrease of the calcein flux. This may suggest in the case of horizontal vibrations that microspike holes are enlarged during vibrations and retract to some extent after removal of the microspikes. In the case of vertical vibrations, the calcein transport may be caused by a pumping effect of the array of microspikes moving up and down. It is also conceivable that vertical vibrations enlarge microspike holes but to a lesser extent than horizontal vibrations. However, the pumping effect of vertical vibrations may be lessened by the fact that epidermis moves along with microspikes which reduces greatly the displacement of the microspikes with respect to epidermis. Horizontal vibrations do not suffer as much from this problem; because epidermis, in the transport chamber, is clamped on the edges, it cannot stretch as much in the horizontal direction as in the vertical direction.

When fluxes of calcein were calculated to investigate the effect of microspikes (either left in epidermis or removed after insertion), these fluxes were calculated across the area covered by the microspikes' arrays (0.0915 cm^2); the microspike-to-microspike spacing was taking into account in this area, although it is assumed that much of the transport occurs in the immediate vicinity of the microspikes. So, if we calculated fluxes of calcein taking into account only the immediate periphery of the microspikes (instead of also taking

the microspike-to-microspike spacing into account), the results would have been increased by a factor of up to 5.

It should also be noticed that very few data were collected for each experimental condition (except for passive diffusion for which 10 data points were collected). This implies that the results presented in this thesis should be interpreted carefully; to obtain statistically significant results and draw stronger conclusions, more data points need to be collected.

Microspikes (whether inserted into epidermis and then removed, vibrated, or coupled with a low voltage) were shown to enhance transport of calcein across epidermis. Since most drugs have a molecular weight of less than 500 g/mol (smaller than that of calcein) and are as permeable or more permeable than calcein, our results suggest that transdermal delivery of drugs can be induced by microspikes. Although "high tech" drugs (e.g. macromolecules such as insulin) were not tried, our results suggest that transport of such macromolecules across epidermis may also be significantly enhanced by microspikes.

These results show that our drug delivery approach is very promising even though the original design of our transdermal drug delivery device may have to be slightly altered; the fact that microspikes embedded in epidermis do not enhance significantly transport suggests that in a successful drug delivery device, microspikes may have to be vibrated or coupled with a voltage or both. However, the use of voltage or vibration may be avoided by replacing microspikes by hollow microneedles. Although hollow microneedles may exhibit less strength than microspikes, the excellent mechanical properties of microspikes lead us to think that hollow microneedles may be sturdy enough to pierce stratum corneum without undergoing significant damage.

CHAPTER VII

CONCLUSION

Arrays of microspikes were fabricated using the Black Silicon Method. Control of the fabrication method was demonstrated by making microspikes of different dimensions and profiles. 140-μm- and 180-μm-tall microspikes were tried on skin; they exhibited excellent mechanical properties: within an array, less than 5% of such microspikes broke at the tip (top 5-10 μm) during penetration of epidermis.

Qualitative and quantitative experiments were performed to investigate the drug delivery capabilities of microspikes. Spectrofluorimetry allowed us to measure precisely the transport of calcein, a fluorescent dye, induced by 180-μm-tall microspikes across epidermis. Channels created in epidermis by inserting and removing microspikes enhanced transport of calcein by two orders of magnitude. The calcein transport enhancement even reached three orders of magnitude when a voltage was applied across epidermis after microspikes had been inserted and removed. Vibrating embedded microspikes horizontally and vertically also proved to enhance calcein transport by two orders of magnitude.

The work presented in this thesis illustrates the great potential of microspikes as transdermal drug delivery devices; not only do microspikes demonstrate great intrinsic strength but also, combined with low voltage, they allow transport enhancement of

molecules through the skin's barrier by a factor of up to 3600. Also, the fabrication method that we used is such that the density of microspikes per skin area can be easily customized within an array to yield the desired level of transport enhancement.

Immediate future work will consist of investigating the transport of macromolecules, such as insulin and bovine serum albumin, caused by microspikes; the effect of the size of the microspikes on the level of transport enhancement will also be studied. The substitution of microspikes by hollow needles should also be attempted.

APPENDIX 1

CLEANROOM

Gowning Requirements

class 10:   class 1000:

    -Hood with mask   -Hood or cap

    -Coverall   -Coverall

    -Booties   -Booties

    -PVC gloves   -PVC gloves

Policies and Procedures

-Keep all hair and ears covered with hood or cap

-Men with beards or mustaches must wear masks in both class 10 and class 1000

areas

-Never open the gown in the cleanroom

-Never touch your skin with your gloves

-Only authorized users may enter the cleanroom unescorted

-Visitors must be escorted by a cleanroom qualified faculty/staff member

-No food or drink is permitted in the cleanroom

-No corrugated cardboard, styrofoam, foam rubber or non-cleanroom paper is

permitted in the cleanroom

-No pencil, erasers or retractable pens are permitted in the cleanroom

APPENDIX 2

FORMULATION OF THE BLACK SILICON METHOD (Jansen, 1995)

1. *Coarse tuning the profile:* Place a piece of Silicon (Si) in the reactor chamber and adjust the preferred power and pressure for an SF_6/O_2 plasma (e.g. 1 W/cm^2, 100 mTorr, 100 sccm SF_6- and 1 sccm O_2-flow). Etch ~ 1 micron of silicon, open the process chamber, and look if the silicon is black. If not, do the same again but increase the oxygen flow. Proceed with this sequence until it is black. If it stays clean, add extra Si in the reactor to increase the loading until the Si appears black. Increasing the oxygen too much, still will give rise to black-, or better gray-, silicon since there exists a positively tapered profile with hardly any under etching (Figure 26).

2. *Cleaning the surface:* After the black silicon regime is found add CHF_3 to the mixture and increase this flow until the wafer is clean again. Too much CHF_3 will make the profiles isotropic (the etch rate is the same in all the directions) and smooth because the CF_x species are scavenging the oxygen radicals which are needed for the blocking layer.

3. *Fine tuning the profile:* Now a wafer with the mask pattern of interest is inserted in the reactor and the etched profile is checked. Add extra silicon into the reactor chamber until the exposed silicon area is the same as in step 1 and 2. Increasing the SF_6 content will create a more isotropic profile. Adding more oxygen will make the profile positively tapered and extra CHF_3 will make it more negatively tapered (Figure 26a). Adding at the

same time O_2 and CHF_3 with the correct balance will create very smooth and nearly vertical walls. Increasing the pressure or decreasing the power will make the profile more positively tapered. In Figures 26a/b the influence of the O_2/CHF_3 flow and the pressure/power on the profile is given.

As can be concluded from Figures 26a/b, vertical walls can be achieved for any pressure, power, O_2-, CHF_3-, or SF_6-flow.
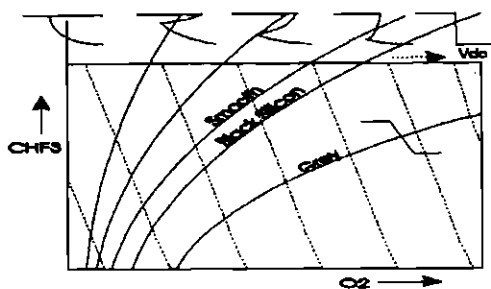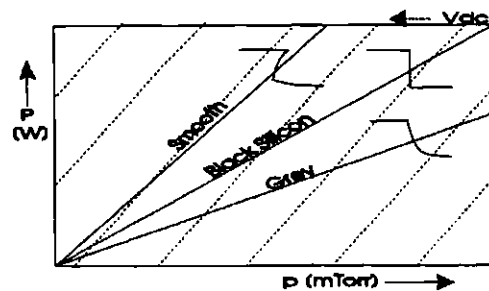

Figure 26a: The Influence Of The Flows On The Profile.

Figure 26b: The Influence Of Power and Pressure On The Profile.

81

APPENDIX 3

SKIN EXPERIMENTS

Sample	Condition	Counts/sec	Counts/sec - PBS	Time (hr)	k	Conc. (M)	Conc. (M) - PBS	Flux (µg/cm²hr)
S+N	S	6.73E+04	4.93E+04	0.25	4.180	6.28E-10	8.89E-10	1.49E-02
	S	5.03E+04	3.23E+04	1	4.180	4.60E-10	5.97E-10	0.00E+00
	S+N	4.71E+04	2.91E+04	1	36.086	4.29E-10	5.41E-10	2.29E-03
	S	8.90E+05	8.82E+05	1	36.086	1.11E-08	1.17E-08	4.07E-01
S+V	S	5.04E+04	3.24E+04	0.25	4.180	4.61E-10	5.99E-10	1.00E-02
	S	5.22E+04	3.42E+04	1	4.180	4.79E-10	6.30E-10	6.31E-04
	S+V	3.93E+05	3.75E+05	1	4.180	4.14E-09	6.01E-09	2.30E-02
	S+V	3.70E+05	3.62E+05	1	4.180	3.25E-09	3.48E-09	0.00E+00
S+N+V	S	8.02E+04	6.22E+04	0.25	4.180	7.57E-10	1.11E-09	1.85E-02
	S	8.53E+04	6.73E+04	1	4.180	8.09E-10	1.19E-09	1.28E-03
	S+N+V	3.39E+06	3.37E+06	1	4.180	4.13E-08	4.75E-08	1.95E-01
	S+V	6.98E+06	6.97E+06	1	36.086	1.99E-07	1.97E-07	5.73E+00
S	S	2.74E+04	9.40E+03	0.25	4.180	2.40E-10	1.87E-10	3.12E-03
	S	6.00E+04	4.20E+04	1	4.180	5.55E-10	7.65E-10	2.57E-03
S	S	1.95E+04	1.50E+03	0.167	4.180	1.67E-10	3.32E-11	8.32E-04
	S	9.03E+04	7.23E+04	1	4.180	8.60E-10	1.27E-09	5.22E-03
	S	1.12E+05	9.40E+04	1	4.180	1.08E-09	1.63E-09	2.56E-03
	S	1.90E+05	1.82E+05	1	4.180	1.90E-09	3.05E-09	7.28E-03
S+N	S	3.34E+05	3.16E+05	0.167	4.180	3.48E-09	5.11E-09	1.28E-01
	S	1.25E+05	1.07E+05	1	4.180	1.22E-09	1.84E-09	0.00E+00
	S+N	1.30E+05	1.12E+05	1	36.086	1.27E-09	1.93E-09	1.62E-02
	S	1.69E+06	1.67E+06	1	36.086	1.96E-08	2.45E-08	8.30E-01
S+N+V	S	2.01E+05	1.83E+05	0.167	4.180	2.02E-09	3.06E-09	7.67E-02
	S	4.37E+05	4.19E+05	1	4.180	4.63E-09	6.67E-09	1.76E-02
	S+N+V	1.00E+07	9.98E+06	1	4.180	1.31E-07	1.32E-07	5.29E-01
	S+V	6.48E+07	6.48E+07	1	36.086	9.66E-07	7.68E-07	2.39E+01

S = epidermis
N = microspikes
V=voltage
k = constant taking area of epidermis into account

HORIZONTAL VIBRATION EXPERIMENTS

Sample		Counts/sec	Counts/sec - PBS	Time (hr)	k	Conc. (M)	Flux (µg/cm²hr)
S+N+Vib	S	1.30E+04	6.87E+03	0.25	4.18	2.17E-10	3.63E-03
	S	2.04E+04	1.43E+04	2	4.18	4.51E-10	5.44E-04
	S+N+Vib	2.46E+06	2.45E+06	1.25	36.086	7.76E-08	2.23E+00
	S+N+Vib	1.90E+06	1.89E+06	1	36.086	5.99E-08	0.00E+00
	S	2.59E+06	2.58E+06	1	36.086	8.18E-08	1.05E+00

S = epidermis
N = microspikes
V = voltage
Vib = vibration
k = constant taking area of epidermis into account

VERTICAL VIBRATION EXPERIMENTS

Sample		Counts/sec	Counts/sec - PBS	Time (hr)	k	Conc. (M)	Flux (µg/cm²hr)
S+N+Vib	S	1.11E+04	4.12E+03	0.25	4.18	1.30E-10	2.18E-03
	S	1.34E+04	6.42E+03	1	4.18	2.03E-10	3.69E-04
	S+N+Vib	6.98E+05	6.91E+05	1	36.086	2.19E-08	7.82E-01
	S	1.05E+06	1.04E+06	1	36.086	3.30E-08	4.97E-01

S = epidermis
N = microspikes
V = voltage
Vib = vibration
k = constant taking area of epidermis into account

REFERENCES

J.A. Bouwstra, M.A. de Vries, G.S. Gooris, J. Brussee and M. Ponec, "Thermodynamic and structural aspect of the skin barrier", Journal of Controlled Release, vol. 15, 1991, pp. 209-220.

S.A. Campbell (au.), "The science and engineering of microelectronic fabrication", Oxford University Press, Oxford, 1996.

Y.W. Chien, "Novel drug delivery systems: fundamentals, developmental concepts, biomedical assessments", Marcel Dekker, New York, 1991.

D.J. Edell, V.V. Toi, V.M. McNeil and L.D Clark, "Factors influencing the biocompatibility of insertable microshafts in cerebral cortex", IEEE Transactions on Biomedical Engineering, vol. 39, no. 6, 1992, pp. 635-643.

P.M. Elias, "Structure and function of the stratum corneum permeability barrier", Drug Development Research, vol. 13, 1988, pp. 97-105.

P.M. Elias, "Epidermal barrier function: intercellular lamellar lipid structures, origin, composition and metabolism", Journal of Controlled Release, vol. 15, 1991, pp. 199-208.

M. Fartasch, "The Nature of the epidermal barrier: structural aspects", Advanced Drug Delivery Reviews, vol. 18, 1996, pp. 273-282.

Y. Gross, "Drug delivery devices", World Intellectual Property Organization, International Publication Number: WO 93/17754, September 16, 1993.

Y. Gross and J.G. Kelly, "Intradermal drug delivery device and method for the intradermal delivery of drugs", U.S. Patent, No. 5 527 288, June 18, 1996.

R. H. Guy, "Current status and future prospects of transdermal drug delivery", Pharmaceutical Research, vol. 13, No. 12, 1996, pp. 1765-1769.

J. Hadgraft and R. Guy (eds.), "Transdermal drug delivery: developmental issues and research initiatives", 1989, New York.

M. Haga, M. Akatani, J. Kikuchi, Y. Ueno, and M. Hayashi, "Transdermal iontophoretic delivery of insulin using a photoetched microdevice", <u>Journal of Controlled Release</u>, vol. 43, 1996, pp. 139-149.

R.C. Jaeger (au.), "Introduction to microelectronic fabrication", Neudeck and Pierret, 1993.

H. Jansen, M. de Boer, B. Otter and M. Elwenspoek, "The black silicon method IV: the fabrication of three dimensional structures in silicon with high aspect ratios for scanning probe microscopy and other applications", <u>Micro Electro Mechanical Systems</u>, 1995, pp. 88-93.

H. Jansen, M. de Boer, B. Otter and M. Elwenspoek, "The black silicon method VI: high aspect ratio trench etching for Mems applications", <u>Micro Electro Mechanical Systems</u>, 1996, pp. 250-257.

H. Jansen, "A survey on the reactive ion etching of silicon in microtechnology", <u>Ph.D. Thesis</u>, University of Twente, The Netherlands, 1996, pp. 2.1-2.14.

G.B. Kasting and L.A. Bowman, "DC electrical properties of frozen, excised human skin", <u>Pharmaceutical Research</u>, vol. 7, 1990, pp. 134-143.

R. Langer, "New methods of drug delivery", <u>Science</u>, No. 249, 1990, pp. 1527-1533.

E. Meehan, Y. Gross, D. Davidson, M. Martin, and I. Tsals, "A microinfusor device for the delivery of therapeutic levels of peptides and macromolecules", <u>Journal of Controlled Release</u>, vol. 46, 1996, pp. 107-116.

U.F. Pliquett, T.E. Zewert, T. Chen, R. Langer, and J.C. Weaver, "Imaging of fluorescent molecule and small ion transport through human stratum corneum during high voltage pulsing: localized transport regions are involved", <u>Biophysical Chemistry</u>, vol. 58, 1996, pp. 185-204.

M.R. Prausnitz, V.G. Bose, R. Langer, and J.C. Weaver, "Electroporation of mammalian skin: a mechanism to enhance transdermal drug delivery", <u>Proceedings of The National Academy of Science, USA</u>, vol. 90, 1993, pp. 10504-10508.

M.R. Prausnitz, C.S. Lee, C.H. Liu, J.C. Pang, T.P. Singh, R. Langer, and J.C. Weaver, "Transdermal transport efficiency during skin electroporation and iontophoresis", <u>Journal of Controlled Release</u>, vol. 38, 1996, pp. 205-217.

J.R. Robinson and V.H. Lee (eds.), "Controlled drug delivery: fundamentals and applications", Marcel Dekker, New York, 1988.

Silicon MicroDevices, "Micromechanical patch for enhancing the delivery of compounds through the skin", World Intellectual Property Organization, International Publication Number: WO 96/37256, July 18, 1993.

E.W. Smith and H.I. Maibach (eds.), "Percutaneous penetration enhancers", CRC Press, Boca Raton, FL, 1995.

R. Vanbever, M.R. Prausnitz, and V. Préat, "Macromolecules as novel transdermal transport enhancers for skin electroporation", Pharmaceutical Research, vol. 14, No. 5, 1997, pp. 638-644.
R. Vanbever, D. Fouchard, A. Jodoul, N. De Morre, V. Préat, and J.-P. Marty "In vivo non-invasive evaluation of hairless rat skin after high-voltage pulse exposure". (submitted).

P.W. Wertz, "The nature of the epidermal barrier: biochemical aspects", Advanced Drug Delivery Reviews, vol. 18, 1995, pp. 283-294.